Backbone Engineering in the Hydrophobic Core of Villin Headpiece

Yuhan Lin, Ryley M. David, Dyllan M. Amin, Shane W. J. Osborne, W. Seth Horne*

Department of Chemistry, University of Pittsburgh, Pittsburgh, PA 15260 (USA)

SUPPORTING INFORMATION

Experimental

Protein synthesis and purification. All proteins were synthesized by Fmoc solid-phase methods on Tentagel XV rink amide resin (0.24 mmol/g), either manually at room temperature (**β³F6**, **β³F10**), manually with microwave heating on a CEM MARS microwave reactor (**HP35**, **β³F17**, **β³L28**, **ACPC28**, **ACPC29** and **ACPC30**), or in automated fashion on a Gyros PurePep Chorus peptide synthesizer (all remaining variants). The choice of method is not essential to the outcome of the synthesis and was made based on instrument availability. All protected amino acid monomers, including those used to introduce artificial residues, were sourced from commercial vendors. For manual synthesis at room temperature, coupling reactions were performed with Fmoc-protected amino acid (5 equiv. relative to resin), HCTU (4.9 equiv.), and DIEA (7.5 equiv.) in NMP (0.1 M final monomer concentration) for 45 min. Fmoc deprotections were performed with 20% (v/v) 4-methylpiperidine in DMF twice for 5 min each. For manual synthesis with microwave heating, coupling reactions were prepared as described above and performed for 6 min (2 min ramp and 4 min hold) at 70°C. Microwave Fmoc deprotections were performed for 4 min (2 min ramp and 2 min hold) at 80°C. For automated synthesis, coupling reactions were performed with Fmoc-protected amino acids (5 equiv. relative to resin), PyOxim (5.5 equiv.), and DIEA (10 equiv.) in DMF (0.1 M final monomer concentration). The reaction was allowed to proceed for 30 min at room temperature, then repeated with fresh reagents. Fmoc deprotections were performed with 20% (v/v) 4-methylpiperidine in DMF twice for 5 min each. Among the non-canonical building blocks, we have found the C_α-Me-α residues can be challenging to couple in some contexts. To mitigate this, protected C_α-Me-α monomers were coupled manually with microwave heating as outlined above using PyAOP in place of HCTU regardless of synthesis method. Resin was washed 3 times with DMF between each step. Following completion of the synthesis, resin was washed sequentially with DMF, DCM and MeOH and dried under vacuum. Cleavage was performed with TFA:H_2O:1,2-ethanedithiol (EDT):triisopropylsilane (TIS) (92.5%:3%:3%:1.5% by volume) for 4 h. The resulting mixture was filtered, and excess TFA was removed under a nitrogen stream. Cold diethyl ether was added to the remaining slurry to precipitate the peptide. Peptide pellet collected after centrifugation and decanting was dried under vacuum for 5 min to remove residual ether prior to dissolution. Crude peptide products were dissolved in a mixture of solvent A (0.1% TFA in H_2O) and solvent B (0.1% TFA in acetonitrile) and purified by preparative HPLC on a Hitachi LaChrom instrument with a Phenomenex Jupiter C18 column (250 x 21.2 mm, 300 Å pore size, 10 μm particle size) through gradient elution. Purity and identity of peptides were confirmed by analytical HPLC on a Hitachi Chromaster instrument with a Phenomenex Jupiter C18 column (250 × 4.6 mm, 300 Å pore size, 5 μm particle size) and ESI MS (Thermo Fisher Q Exactive Orbitrap instrument) (Figures S2-S14). Purified peptide samples were lyophilized prior to subsequent experiments.

Circular dichroism (CD) spectroscopy. CD experiments were performed on an Olis DSM17 spectrophotometer. Peptide samples were dissolved in water, and concentrations were determined by UV absorbance of tryptophan at 280 nm.[1] Samples for CD analysis consisted of 50 μM peptide in 50 mM phosphate buffer at pH 7.0. CD spectra were acquired with a 1 nm increment and 3 s averaging time. Mean residue ellipticities were corrected by corresponding cell-matched buffer blanks and baseline subtraction. CD scans were acquired at 20°C in the range 190-260 nm. Thermal denaturation experiments were carried out in the range 4-98°C with a 2°C increment (0.05°C dead band) and 2 min equilibration at each temperature and monitored at 222 nm. Thermal unfolding data were fit to a two-state unfolding model to obtain reported T_m values.[2,3] The heat capacity change for unfolding and linear dependence of unfolded baseline ellipticity as a function of temperature were set to zero in the fits.

Fluorescence spectroscopy. Samples of 10 μM peptide in 50 mM pH 7.0 phosphate buffer containing 0-6 M guanidinium hydrochloride (GuHCl) with a 0.2 M increment were prepared in triplicate

and transferred to a 384-well plate. Fluorescence was measured on a Tecan Infinite M1000 Pro microplate reader with an excitation wavelength at 280 nm and emission recorded at 310-400 nm in 1 nm increments (75 flashes per wavelength, 75 μs integration time, 1000 ms settle time). The ratio of intensity at 345 nm (average of 343-347 nm) to intensity at 398 nm (average of 396-400 nm) was calculated and fit to a two-state unfolding model to obtain reported $\Delta G°_{fold}$ values.[4]

NMR data acquisition and structure calculation. All NMR experiments were conducted on a Bruker Avance 700 MHz spectrometer. NMR samples were prepared with 0.9-1 mM peptide, 0.2 mM sodium trimethylsilylpropanesulfonate (DSS) in H_2O:D_2O (9:1) and pH adjusted to ~5 (4.7-5.1). Samples were centrifuged to remove any solid, and the supernatant used for the measurement. Spectra were acquired at 293 K for **HP35** and **α^{Me}F6**, 288 K for **ACPC28**, **ACPC29**, **ACPC30** and **α^{Me}F17**, 283 K for **β^3L28**, 278 K for **β^3K29** and **β^3F6**, and 298 K for **α^{Me}F6/α^{Me}F17/ACPC29**. A 1-dimensional ^{1}H and 2-dimensional homonuclear NOESY (150 ms mixing time), TOCSY (70 ms mixing time), and COSY spectra were acquired for each variant. 2-Dimensional experiments employed 2048 data points in the direct dimension and 512 data points in the indirect dimension. Data were processed using Topspin and calibrated to DSS. Resonances were assigned manually using the software package POKY.[5] NMR structure determination was performed by simulated annealing using the program ARIA (Ambiguous Restraints for Iterative Assignment, version 2.3) in conjunction with Crystallography & NMR System (CNS, version 1.21).[6,7] Run parameters were modified to improve convergence as previously described.[8,9] H-bond restraints for helical regions were generated based on manual inspection of medium-range NOEs. All other NOE distance restraints were generated automatically by the ARIA program. Topology and parameter definitions for the artificial monomers and associated links were manually patched into the open-source CNS/ARIA program using information for analogous canonical residues already present in the distributed files. The set of ten lowest energy structures resulting from each calculation was taken as the NMR ensemble for that variant. Ensemble coordinates and additional experimental data are deposited in PDB and BRMB. Accession codes and structure calculation statistics are provided in Tables S1-S9.

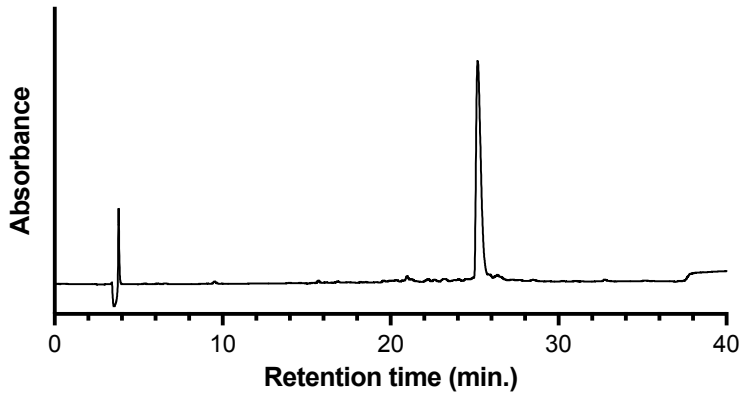

Figure S1. Representative crude analytical HPLC (25-50% solvent B over 30 min) for variant **α^{Me}F6/α^{Me}F17/ACPC29** after TFA cleavage from resin and before purification.

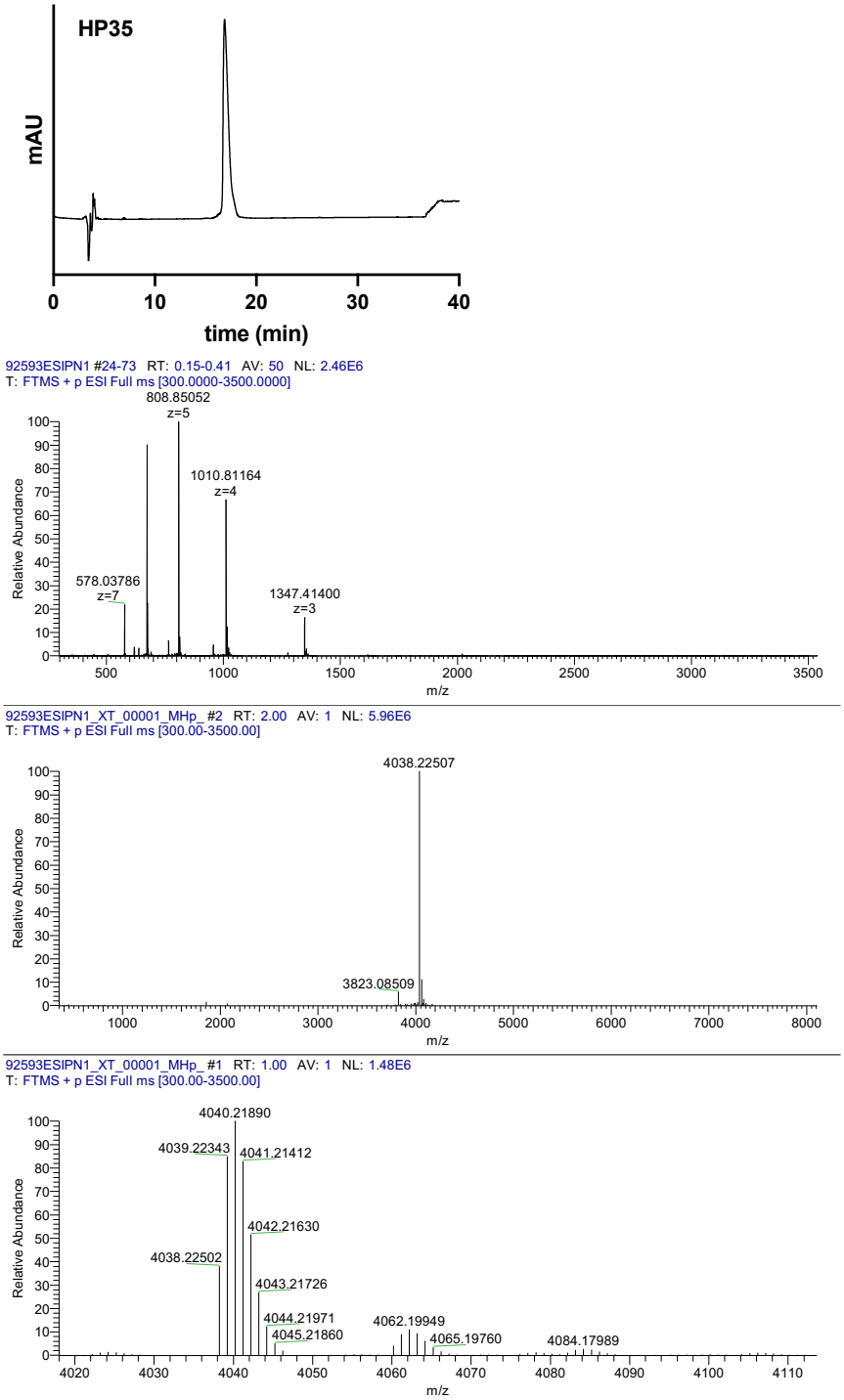

Figure S2. Analytical HPLC (33-43% solvent B over 30 min) and ESI-MS data (top: raw spectrum; middle: deconvoluted spectrum; bottom: zoomed view of deconvoluted spectrum) for purified **HP35**. $[M+H]^+$ calc. is 4040.2022 Da for the most abundant isotope.

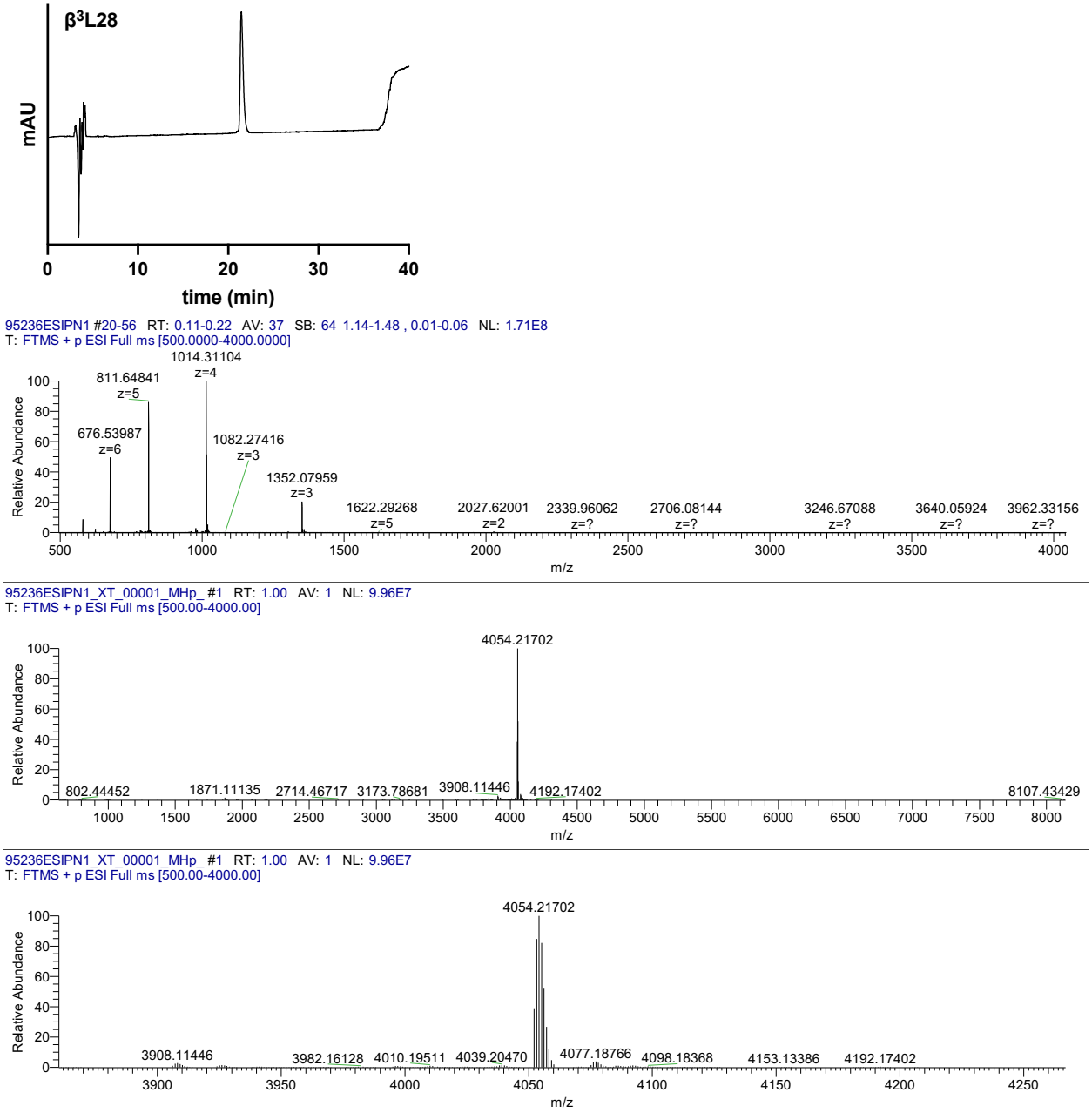

Figure S3. Analytical HPLC (32-42% solvent B over 30 min) and ESI-MS data (top: raw spectrum; middle: deconvoluted spectrum; bottom: zoomed view of deconvoluted spectrum) for purified **β^{3}L28**. $[M+H]^+$ calc. is 4054.2178 Da for the most abundant isotope.

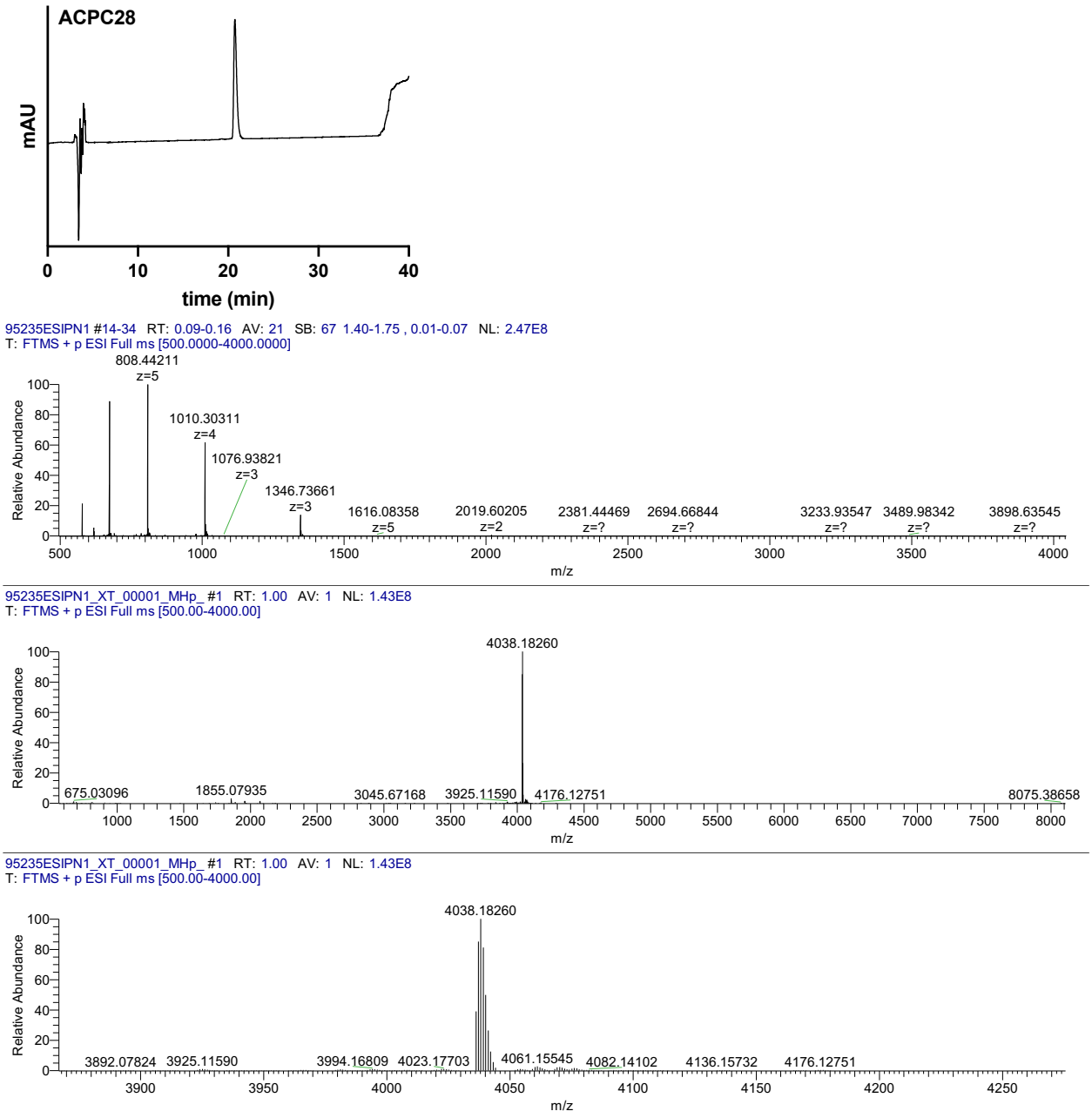

Figure S4. Analytical HPLC (32-42% solvent B over 30 min) and ESI-MS data (top: raw spectrum; middle: deconvoluted spectrum; bottom: zoomed view of deconvoluted spectrum) for purified **ACPC28**. $[M+H]^+$ calc. is 4038.1865 Da for the most abundant isotope.

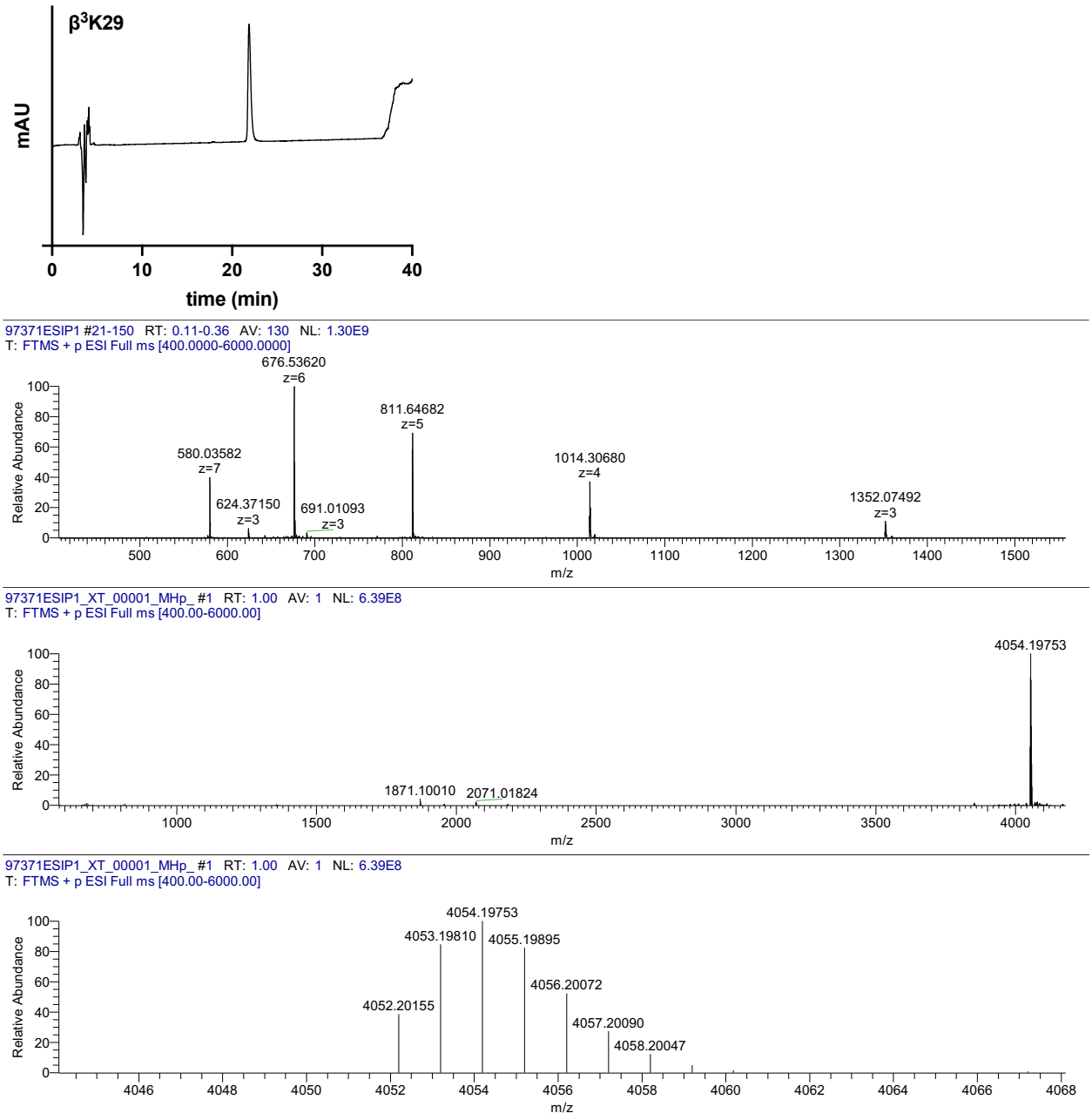

Figure S5. Analytical HPLC (32-42% solvent B over 30 min) and ESI-MS data (top: raw spectrum; middle: deconvoluted spectrum; bottom: zoomed view of deconvoluted spectrum) for purified **β^{3}K29**. $[M+H]^+$ calc. is 4054.2178 Da for the most abundant isotope.

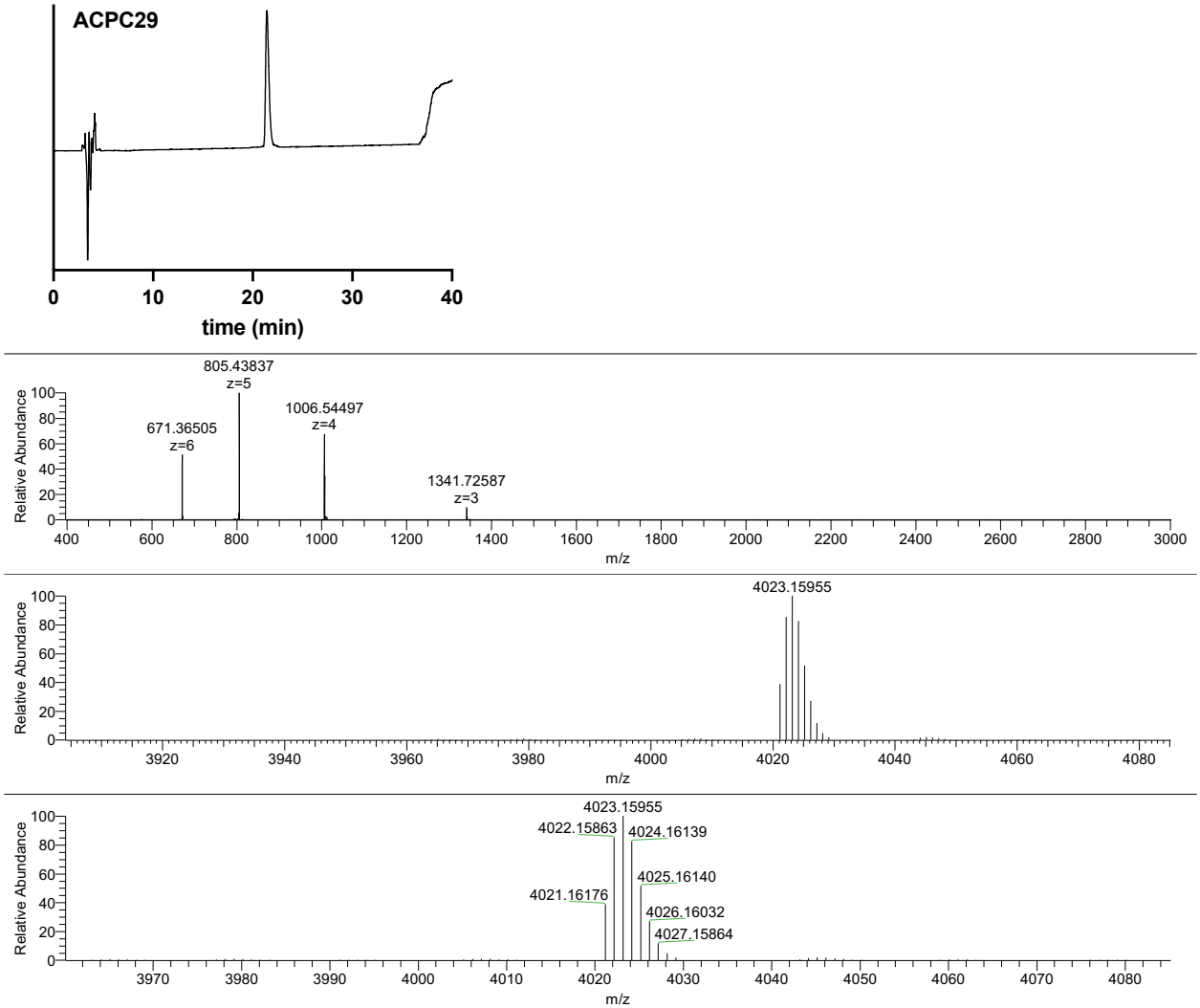

Figure S6. Analytical HPLC (32-42% solvent B over 30 min) and ESI-MS data (top: raw spectrum; middle: deconvoluted spectrum; bottom: zoomed view of deconvoluted spectrum) for purified **ACPC29**. $[M+H]^+$ calc. is 4023.1756 Da for the most abundant isotope.

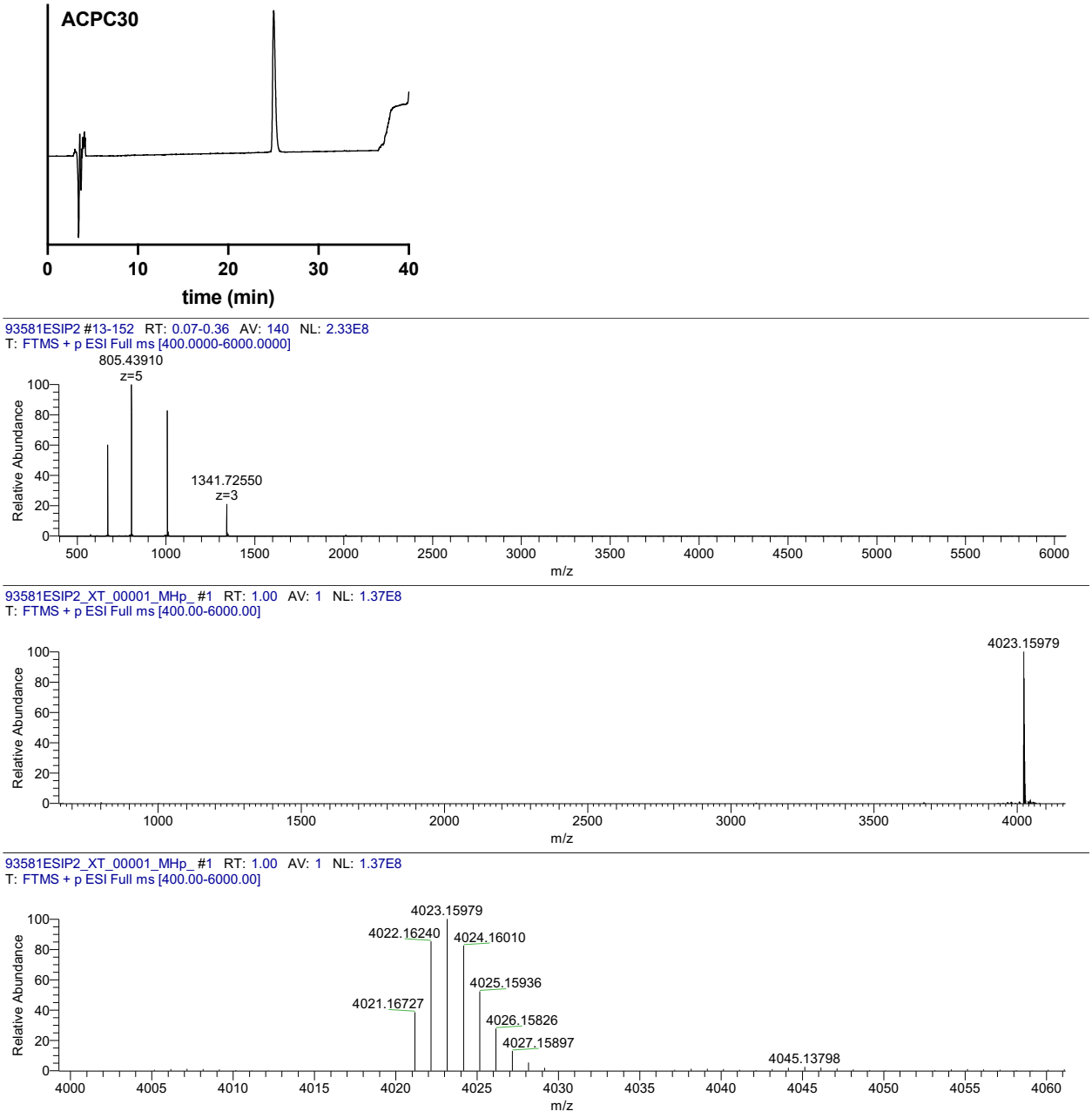

Figure S7. Analytical HPLC (32-42% solvent B over 30 min) and ESI-MS data (top: raw spectrum; middle: deconvoluted spectrum; bottom: zoomed view of deconvoluted spectrum) for purified **ACPC30**. $[M+H]^+$ calc. is 4023.1756 Da for the most abundant isotope.

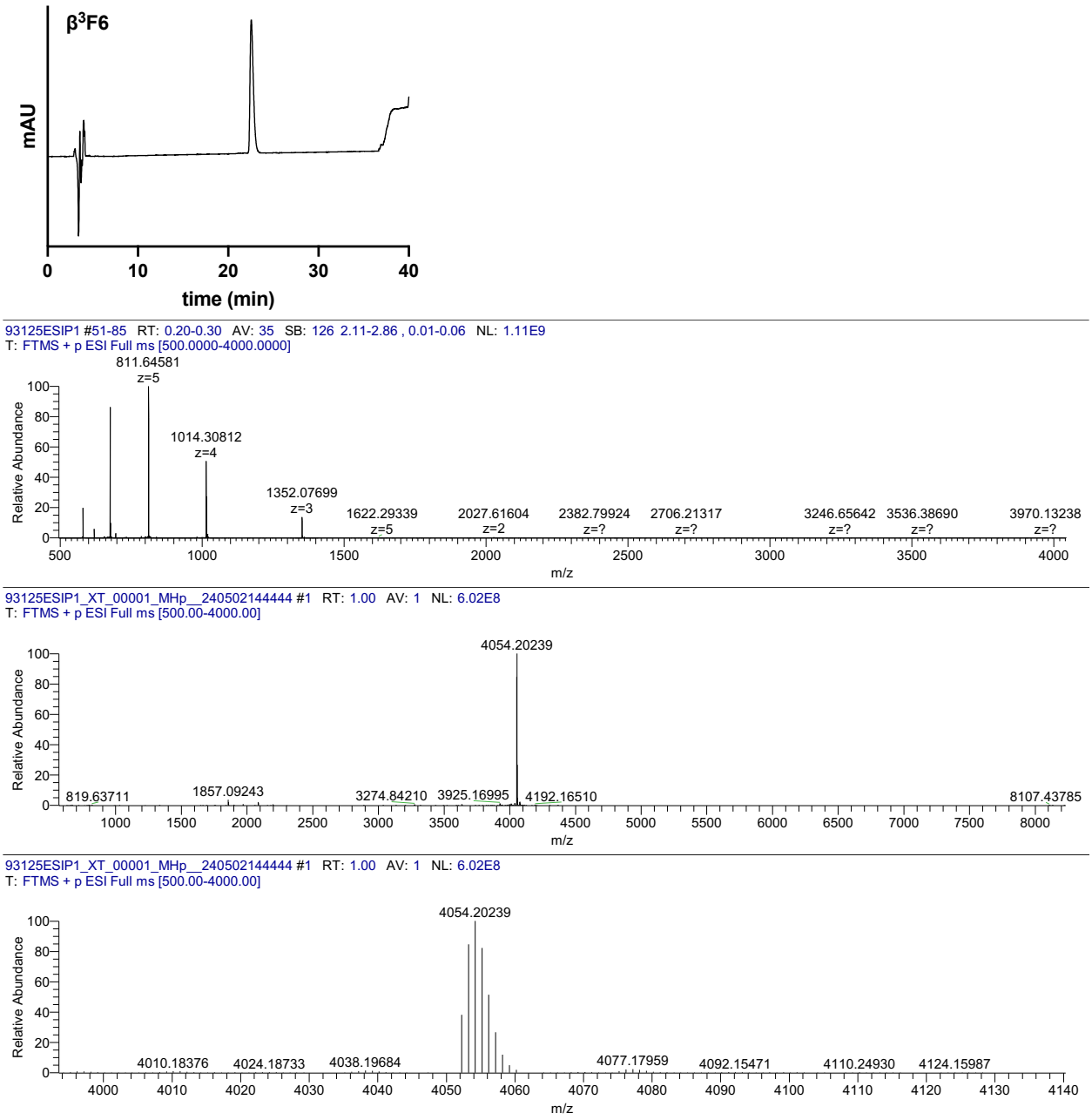

Figure S8. Analytical HPLC (33-43% solvent B over 30 min) and ESI-MS data (top: raw spectrum; middle: deconvoluted spectrum; bottom: zoomed view of deconvoluted spectrum) for purified **β^{3}F6**. $[M+H]^+$ calc. is 4054.2178 Da for the most abundant isotope.

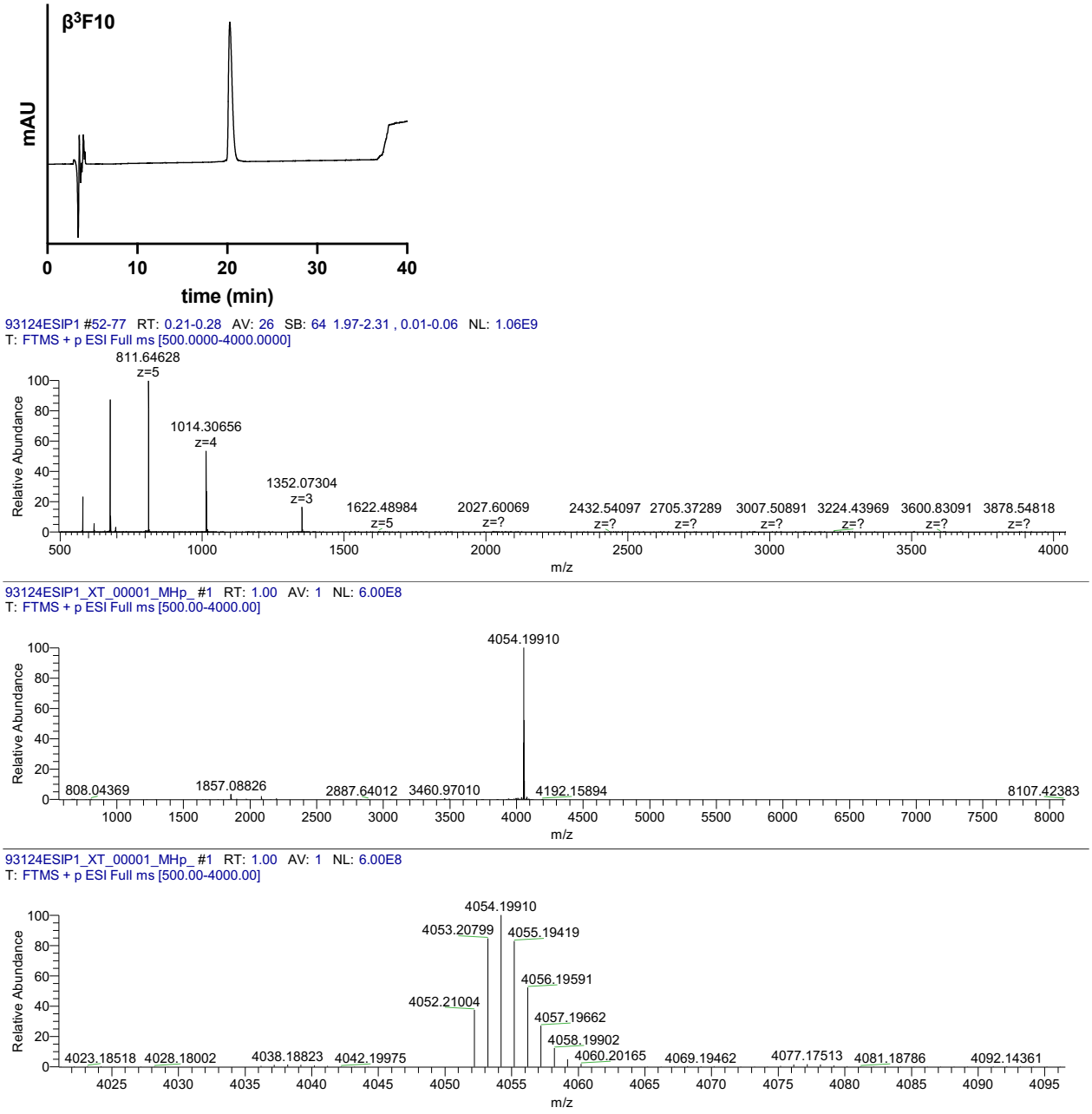

Figure S9. Analytical HPLC (35-45% solvent B over 30 min) and ESI-MS data (top: raw spectrum; middle: deconvoluted spectrum; bottom: zoomed view of deconvoluted spectrum) for purified **β^{3}F10**. $[M+H]^+$ calc. is 4054.2178 Da for the most abundant isotope.

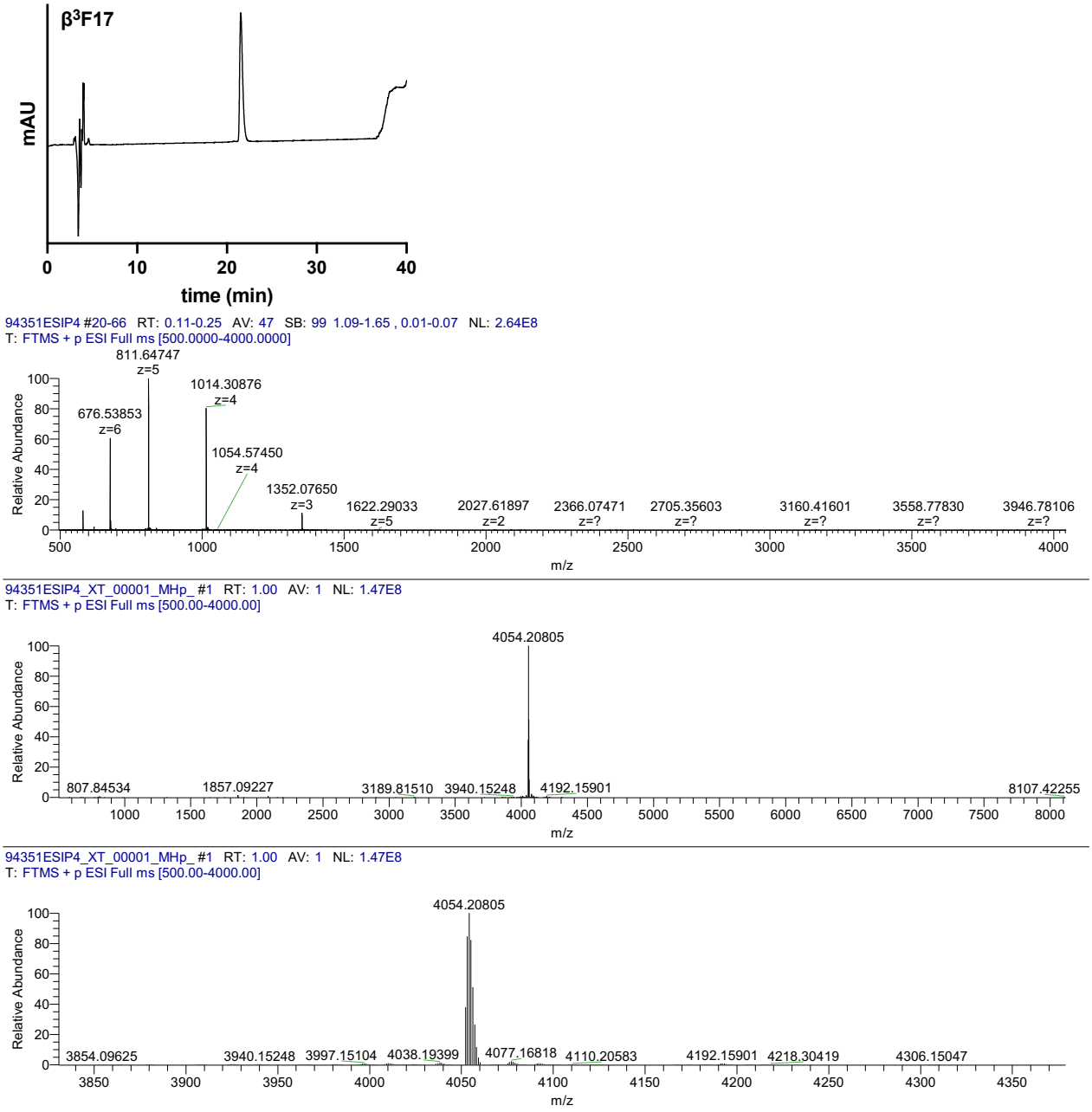

Figure S10. Analytical HPLC (32-42% solvent B over 30 min) and ESI-MS data (top: raw spectrum; middle: deconvoluted spectrum; bottom: zoomed view of deconvoluted spectrum) for purified **β^{3}F17**. $[M+H]^+$ calc. is 4054.2178 Da for the most abundant isotope.

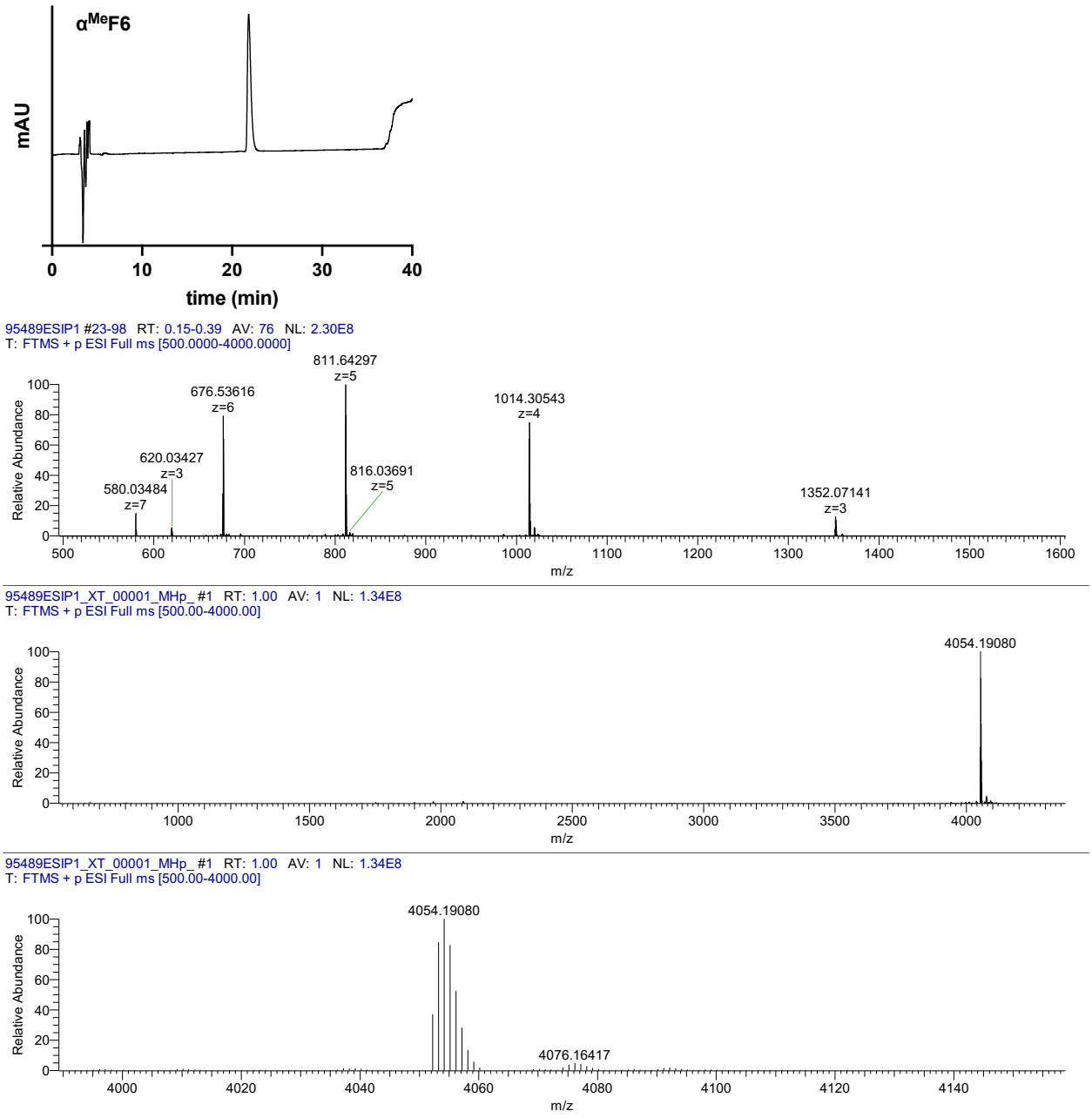

Figure S11. Analytical HPLC (32-42% solvent B over 30 min) and ESI-MS data (top: raw spectrum; middle: deconvoluted spectrum; bottom: zoomed view of deconvoluted spectrum) for purified **α^{Me}F6**. $[M+H]^+$ calc. is 4054.2178 Da for the most abundant isotope.

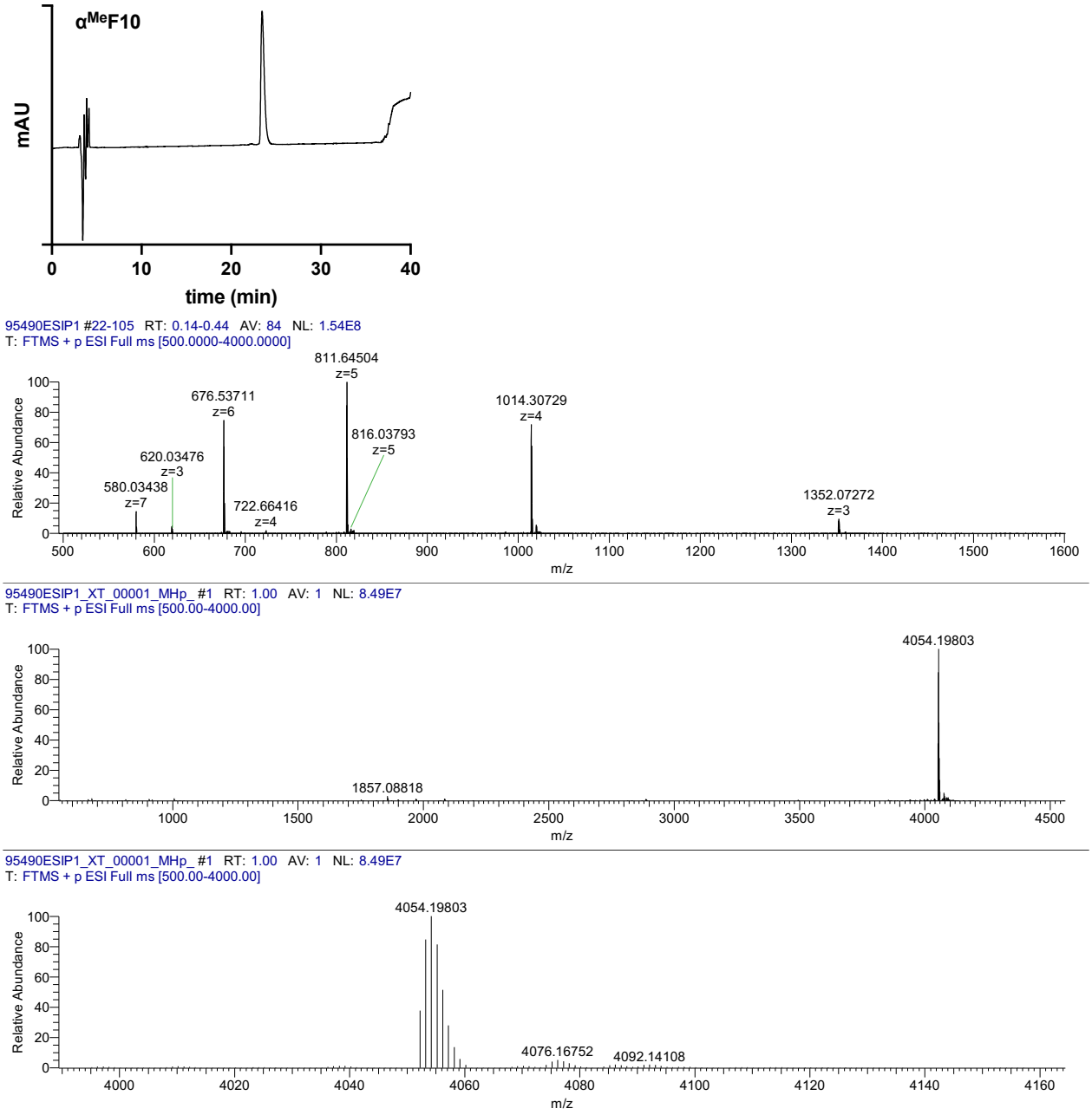

Figure S12. Analytical HPLC (32-42% solvent B over 30 min) and ESI-MS data (top: raw spectrum; middle: deconvoluted spectrum; bottom: zoomed view of deconvoluted spectrum) for purified **α^{Me}F10**. $[M+H]^+$ calc. is 4054.2178 Da for the most abundant isotope.

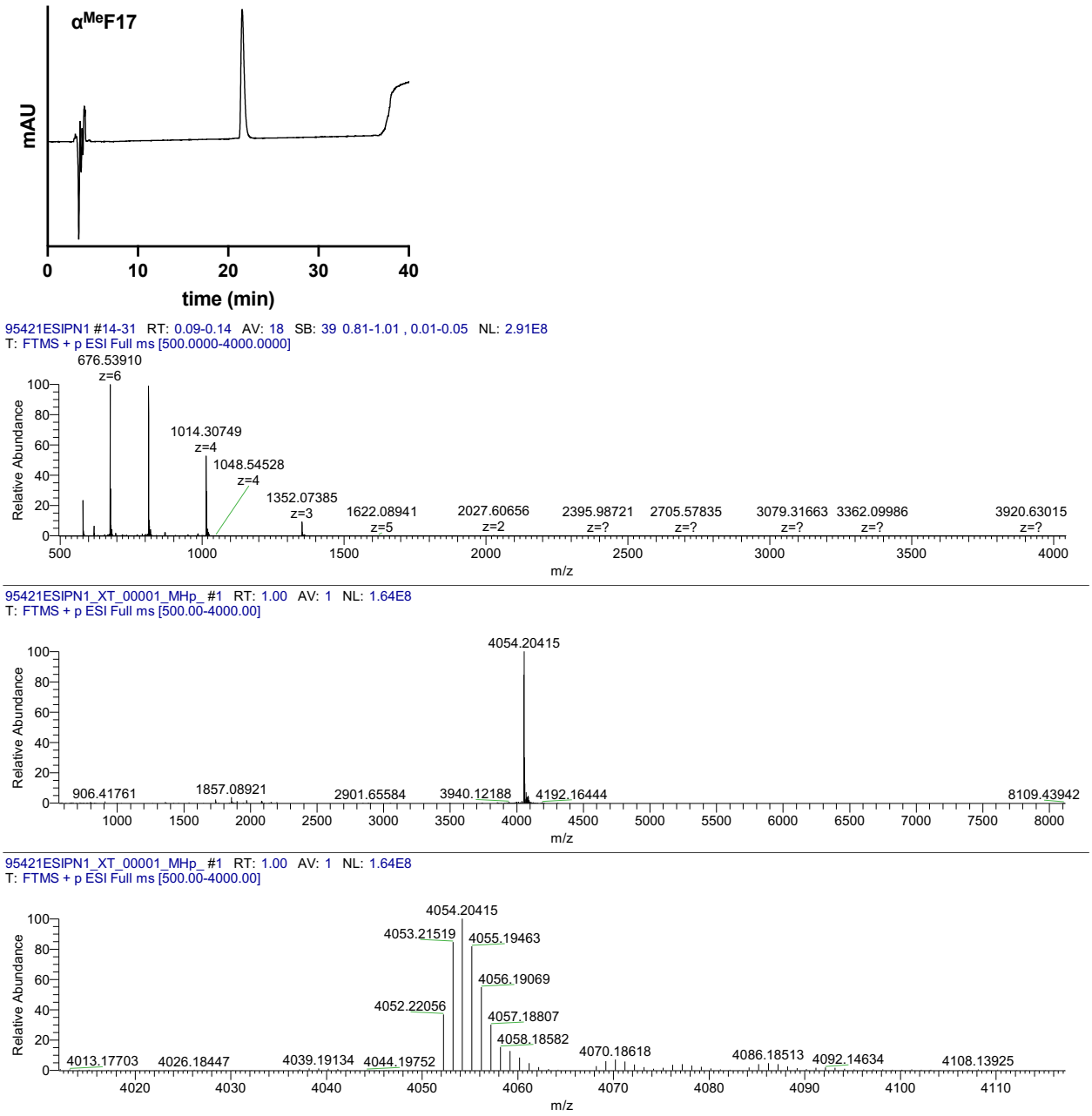

Figure S13. Analytical HPLC (32-42% solvent B over 30 min) and ESI-MS data (top: raw spectrum; middle: deconvoluted spectrum; bottom: zoomed view of deconvoluted spectrum) for purified **α^{Me}F17**. $[M+H]^+$ calc. is 4054.2178 Da for the most abundant isotope.

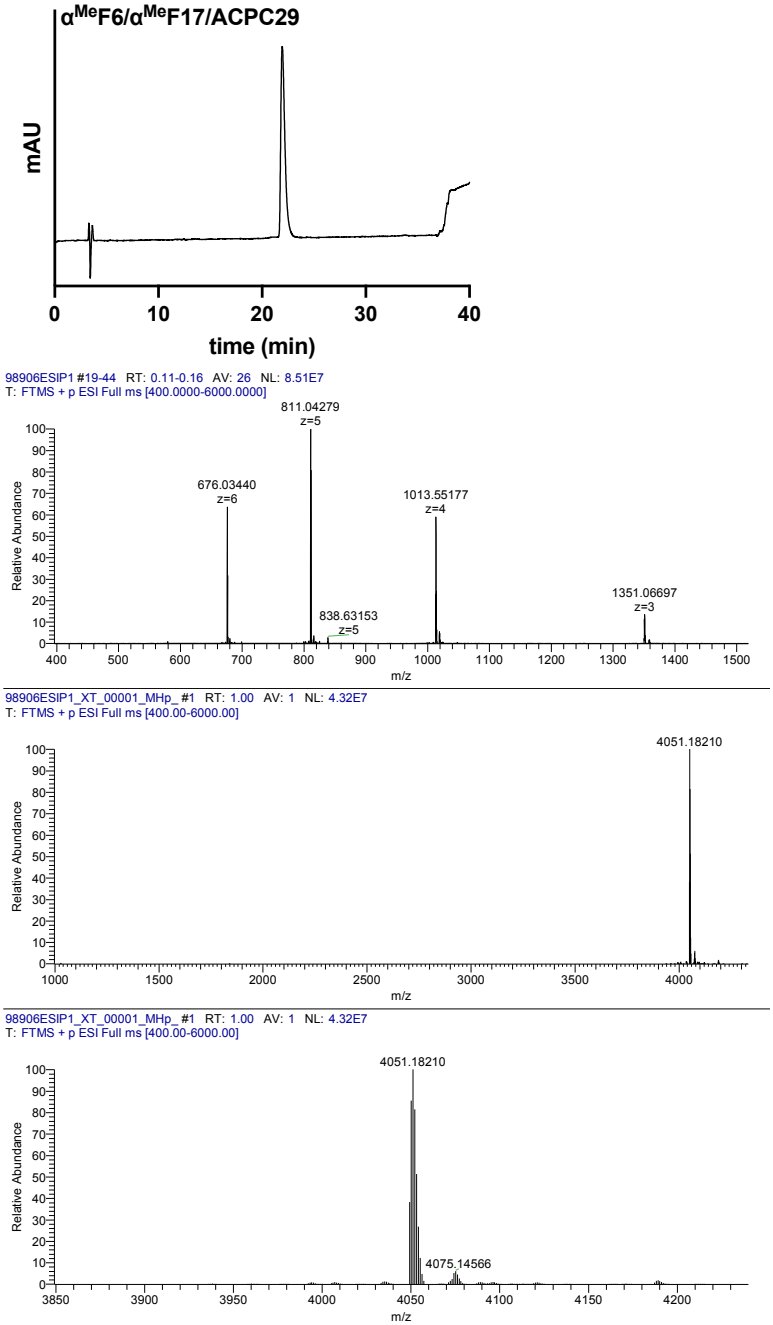

Figure S14. Analytical HPLC (33-43% solvent B over 30 min) and ESI-MS data (top: raw spectrum; middle: deconvoluted spectrum; bottom: zoomed view of deconvoluted spectrum) for purified **α^{Me}F6/α^{Me}F17/ACPC29**. $[M+H]^+$ calc. is 4051.2070 Da for the most abundant isotope.

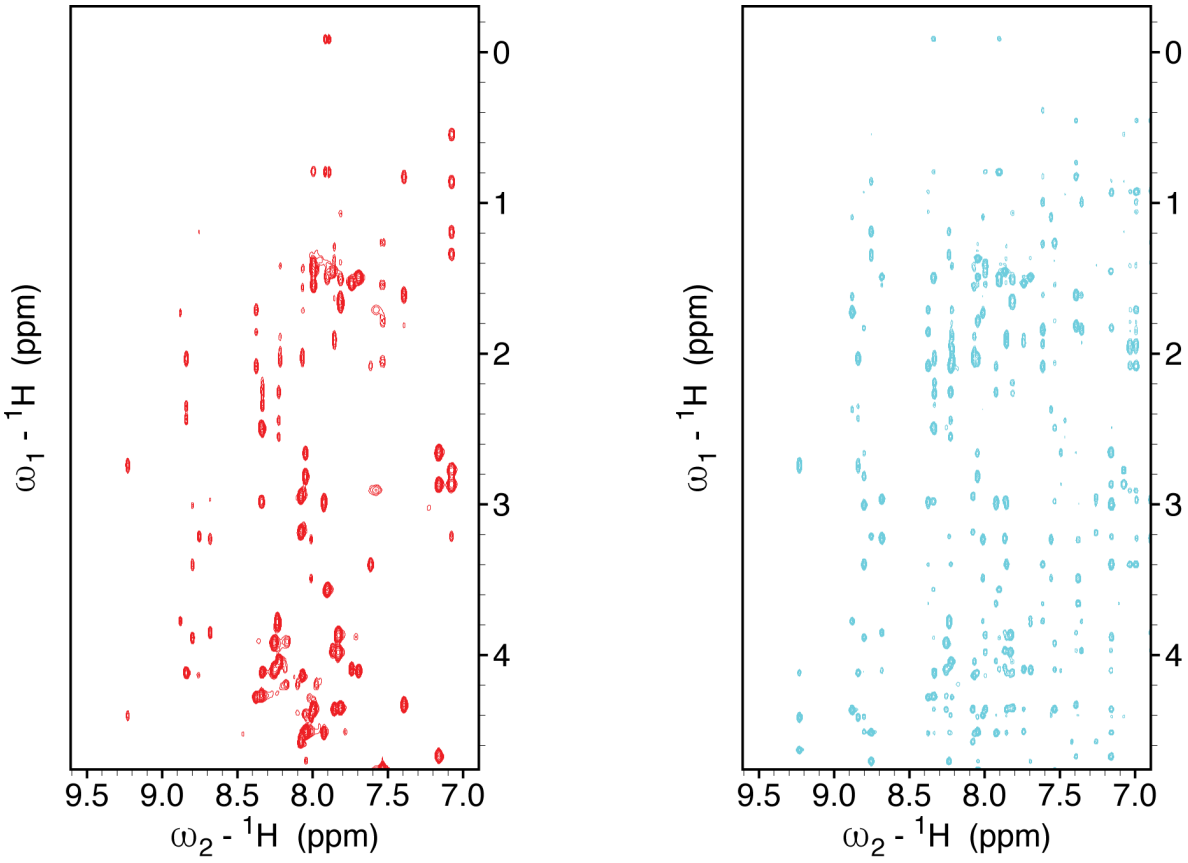

Figure S15. Views of the amide/aromatic to aliphatic region from TOCSY (left) and NOESY (right) spectra of **HP35**. These data are previously published[10] and included here for comparison with variants below.

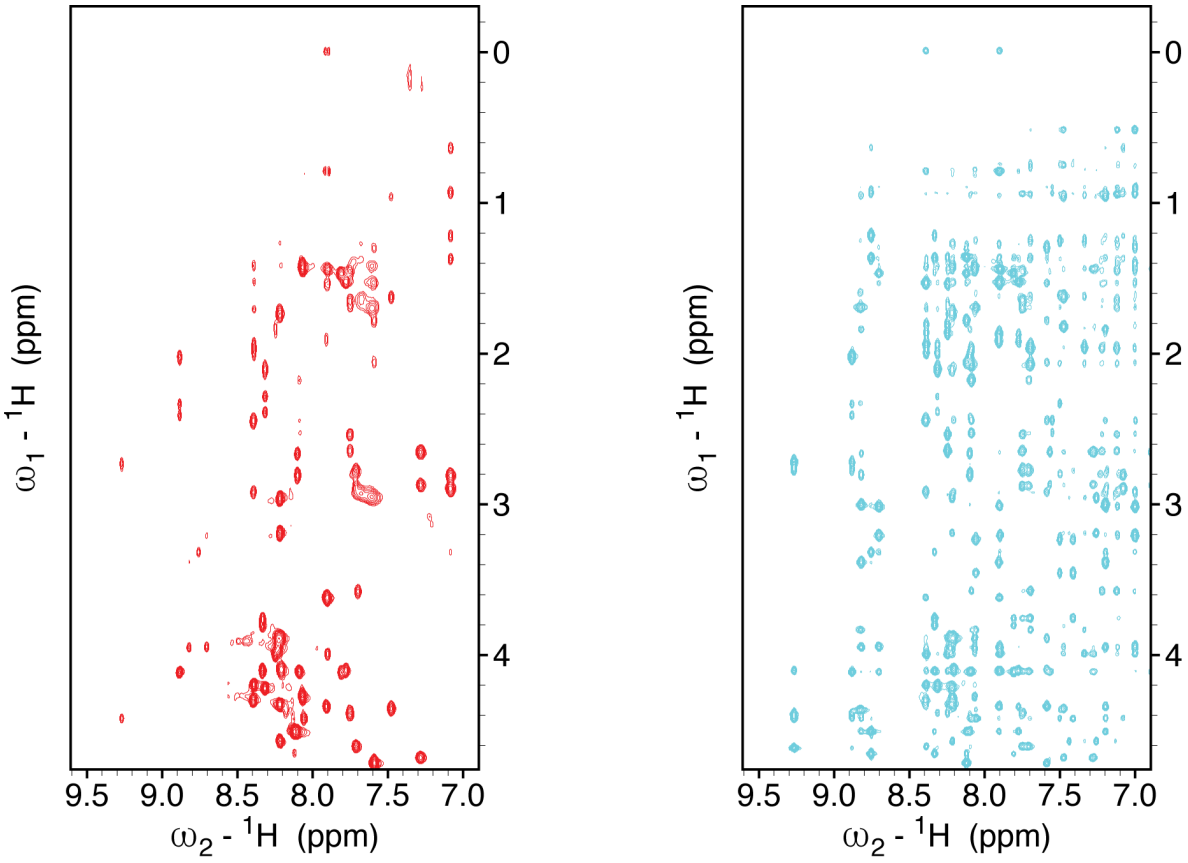

Figure S16. Views of the amide/aromatic to aliphatic region from TOCSY (left) and NOESY (right) spectra of **β^{3}L28**.

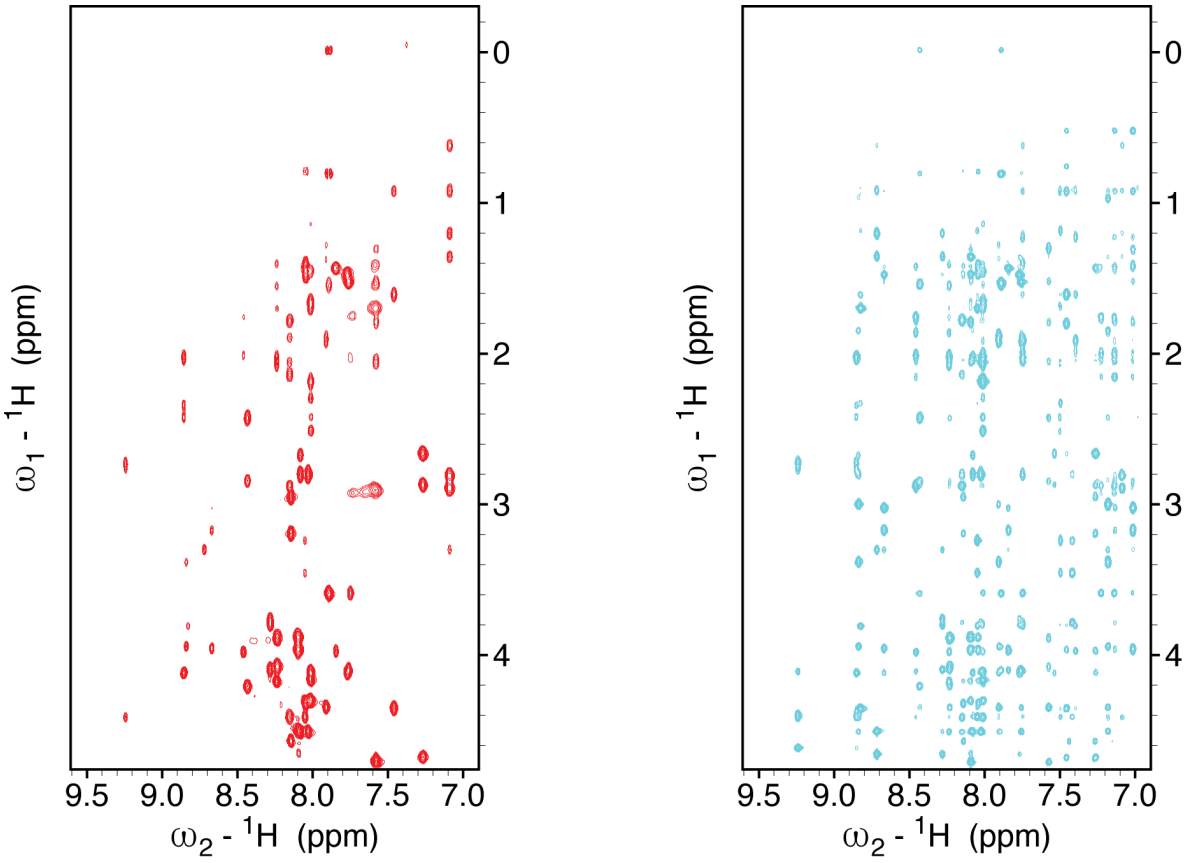

Figure S17. Views of the amide/aromatic to aliphatic region from TOCSY (left) and NOESY (right) spectra of **ACPC28**.

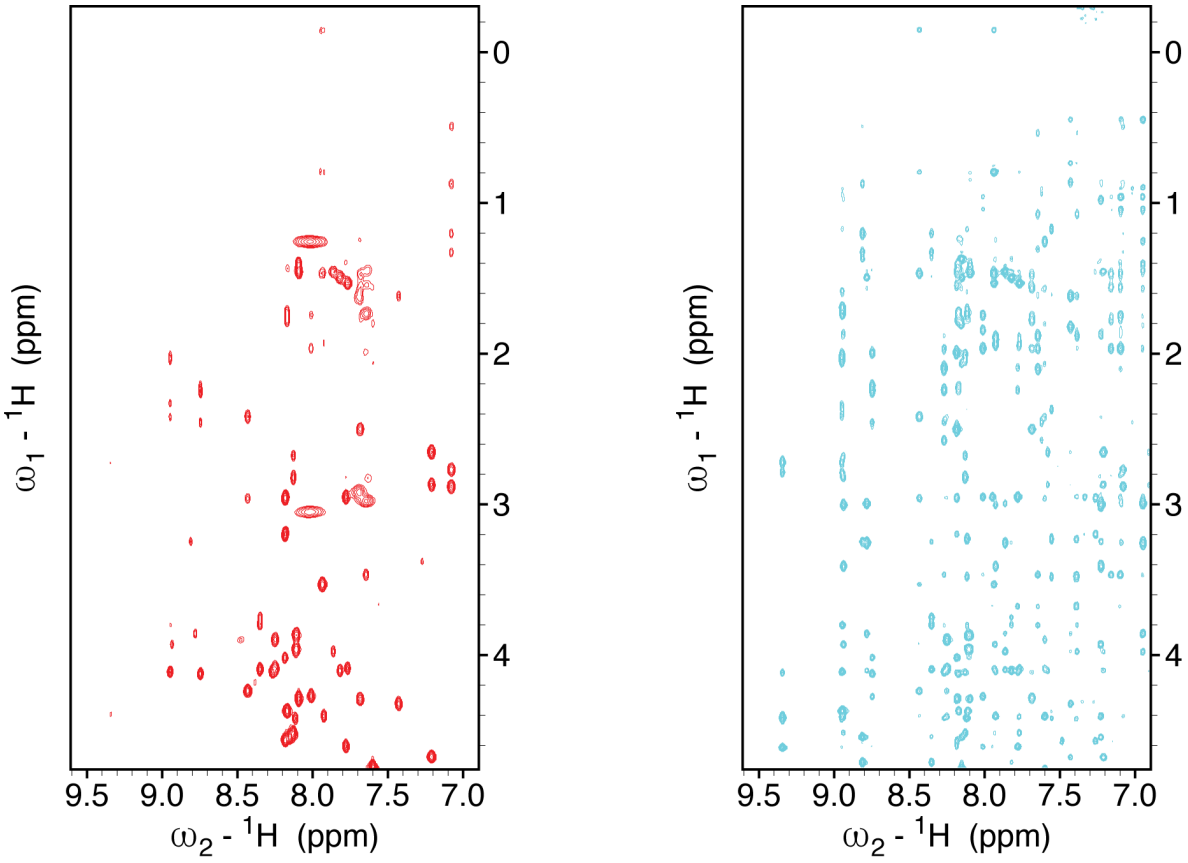

Figure S18. Views of the amide/aromatic to aliphatic region from TOCSY (left) and NOESY (right) spectra of **β³K29**.

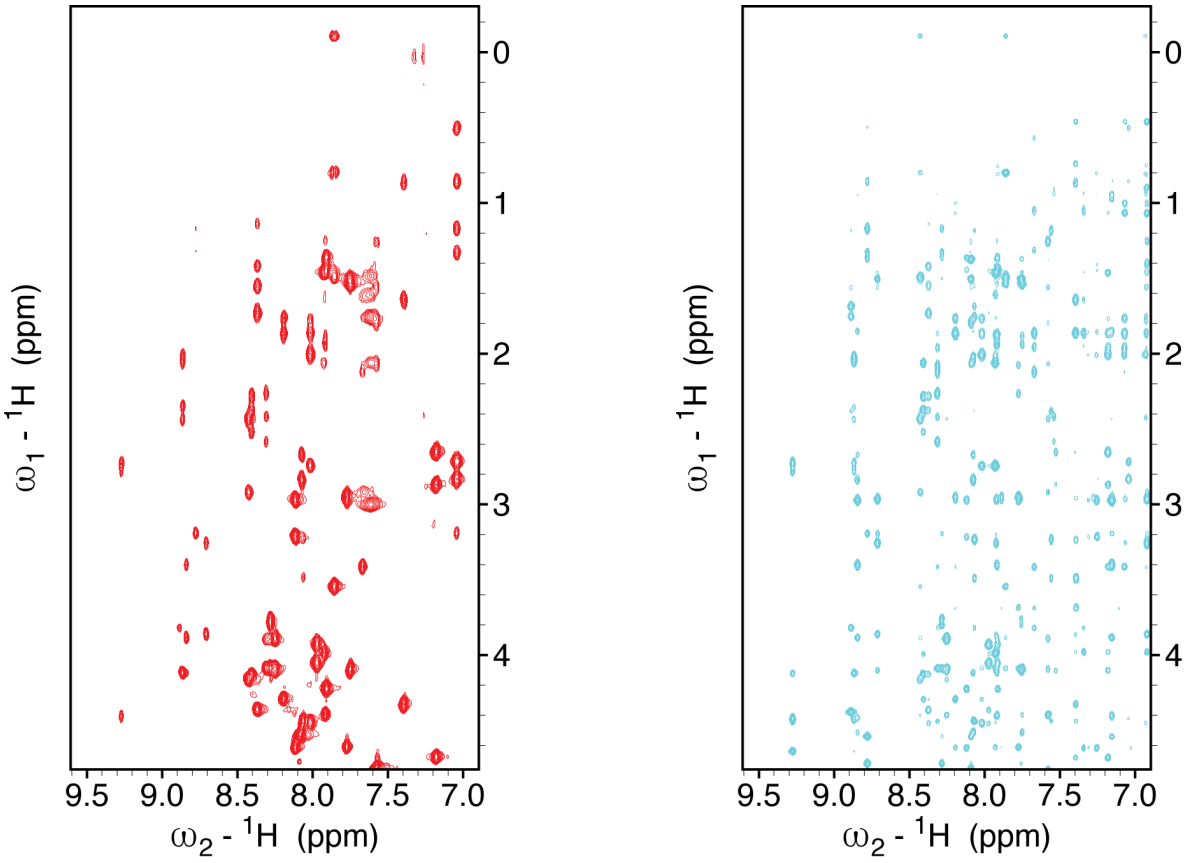

Figure S19. Views of the amide/aromatic to aliphatic region from TOCSY (left) and NOESY (right) spectra of **ACPC29**.

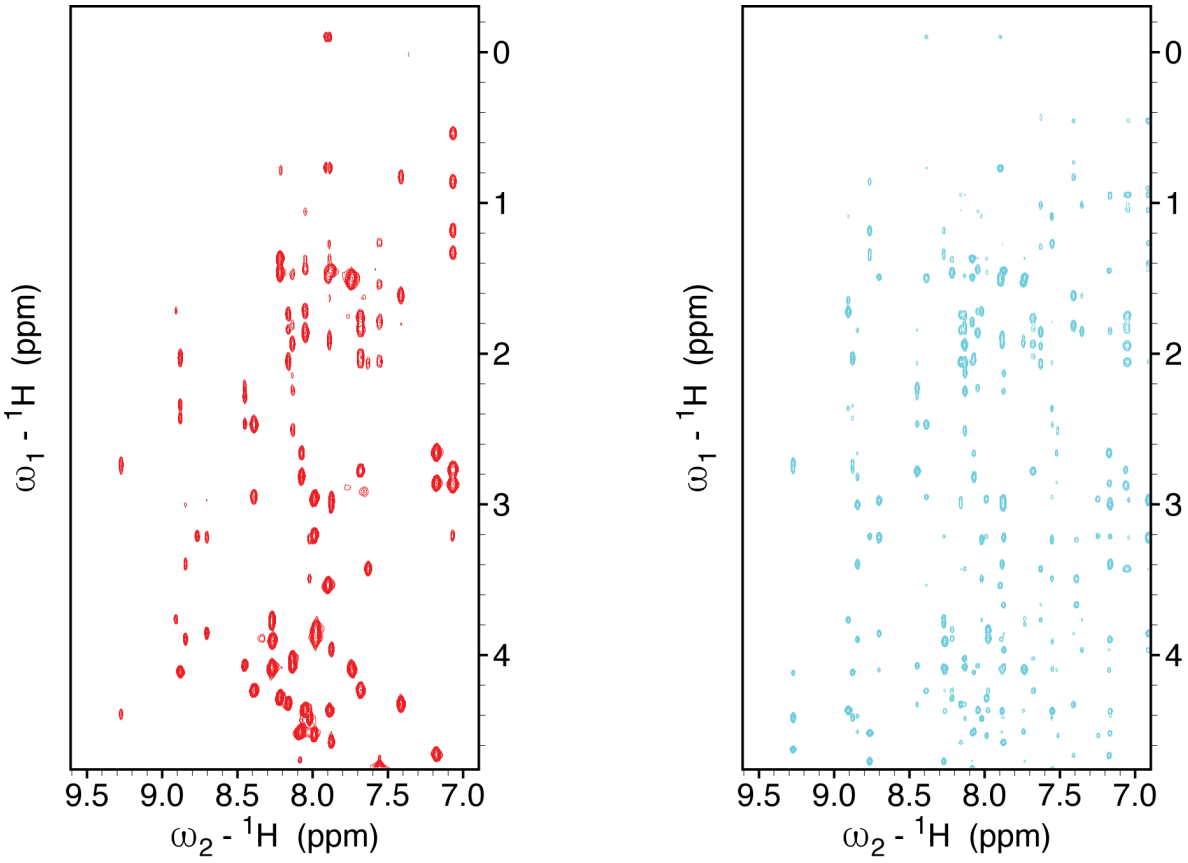

Figure S20. Views of the amide/aromatic to aliphatic region from TOCSY (left) and NOESY (right) spectra of **ACPC30**.

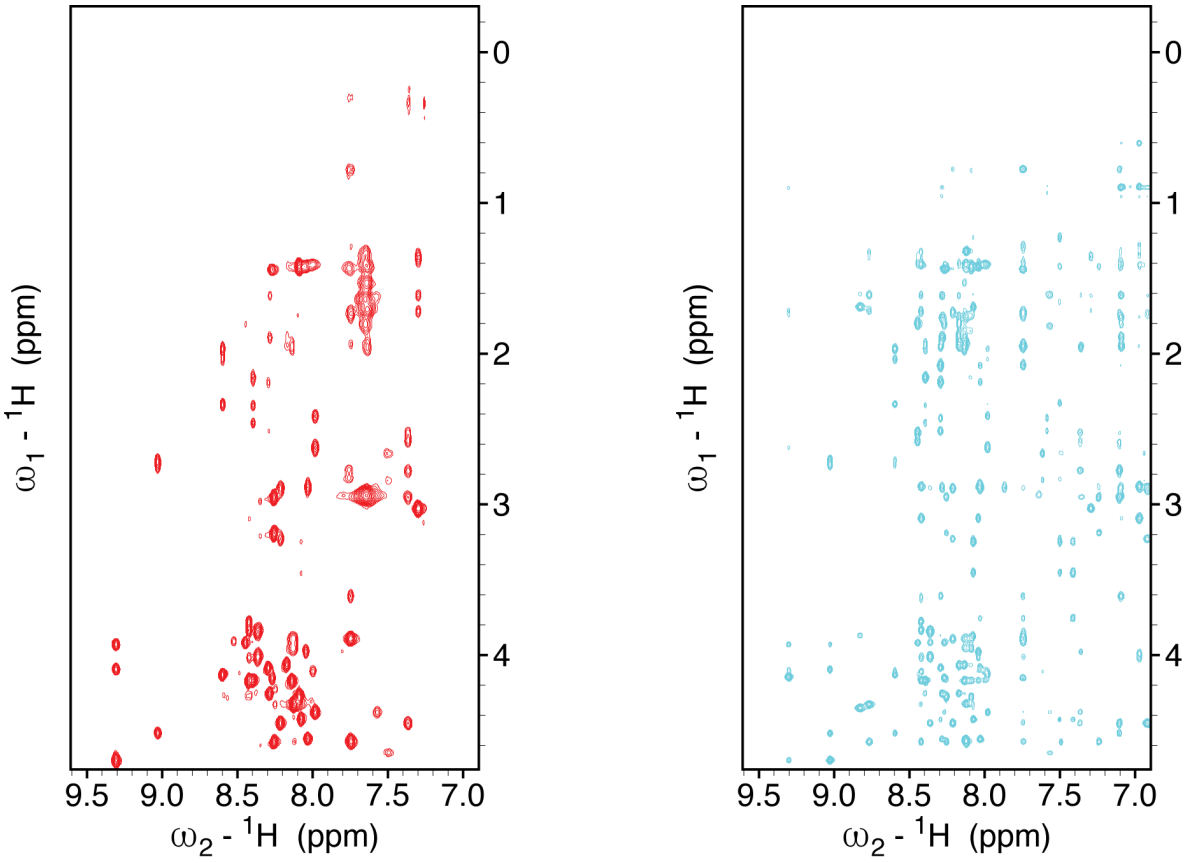

Figure S21. Views of the amide/aromatic to aliphatic region from TOCSY (left) and NOESY (right) spectra of **β³F6**.

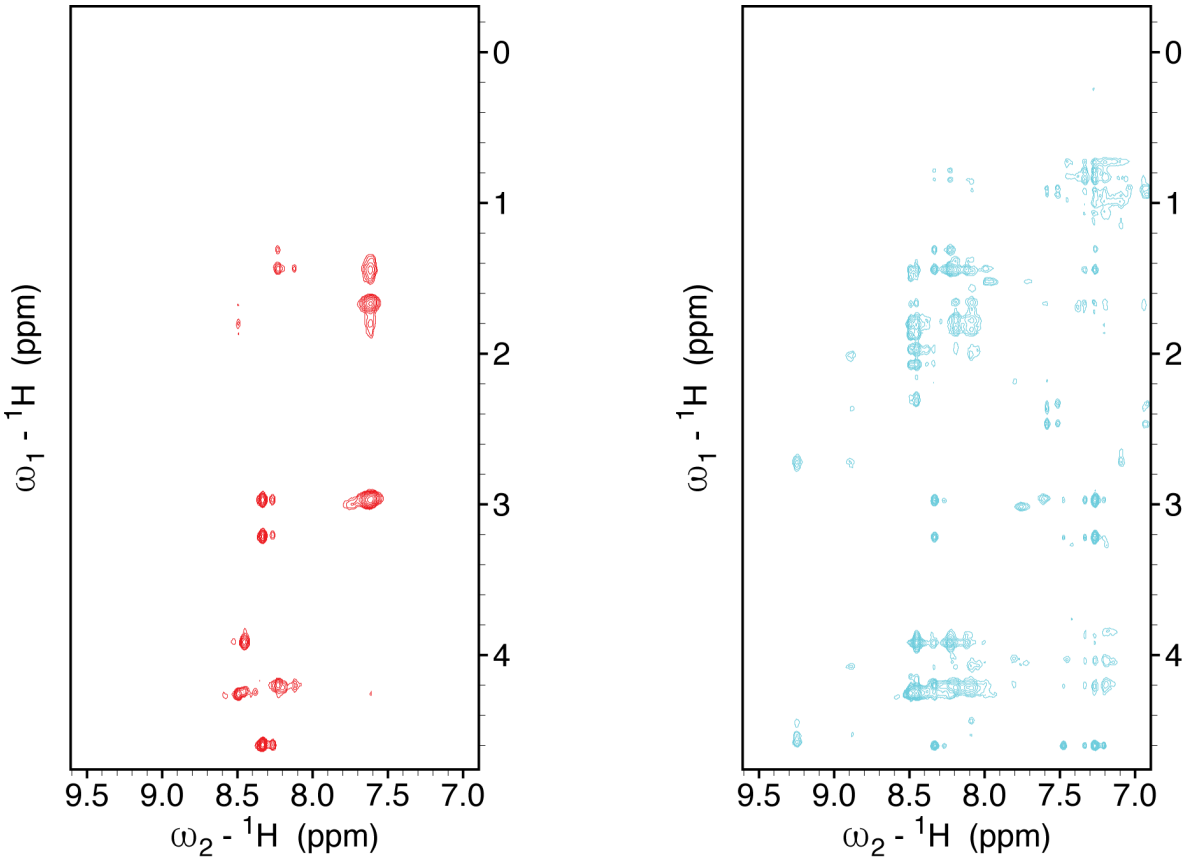

Figure S22. Views of the amide/aromatic to aliphatic region from TOCSY (left) and NOESY (right) spectra of **β³F10**.

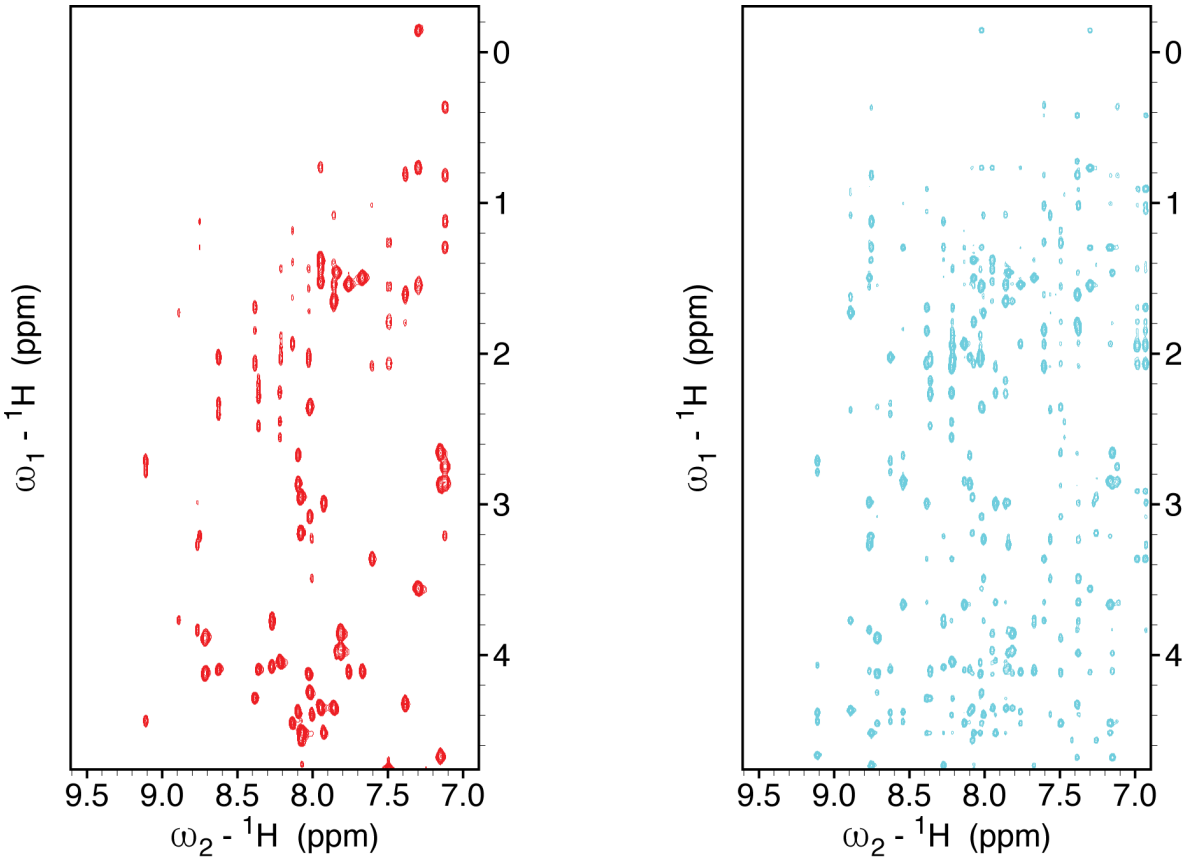

Figure S23. Views of the amide/aromatic to aliphatic region from TOCSY (left) and NOESY (right) spectra of **α^{Me}F6**.

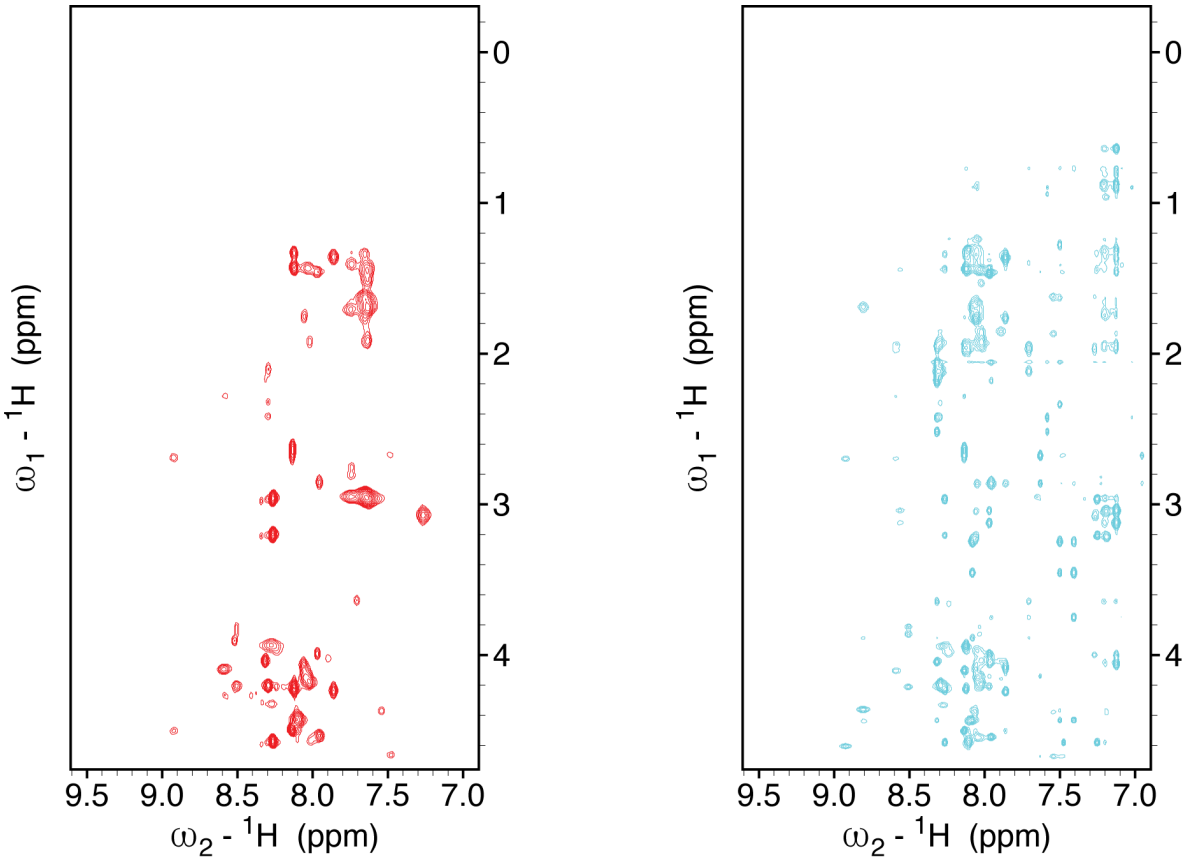

Figure S24. Views of the amide/aromatic to aliphatic region from TOCSY (left) and NOESY (right) spectra of **α^{Me}F10**.

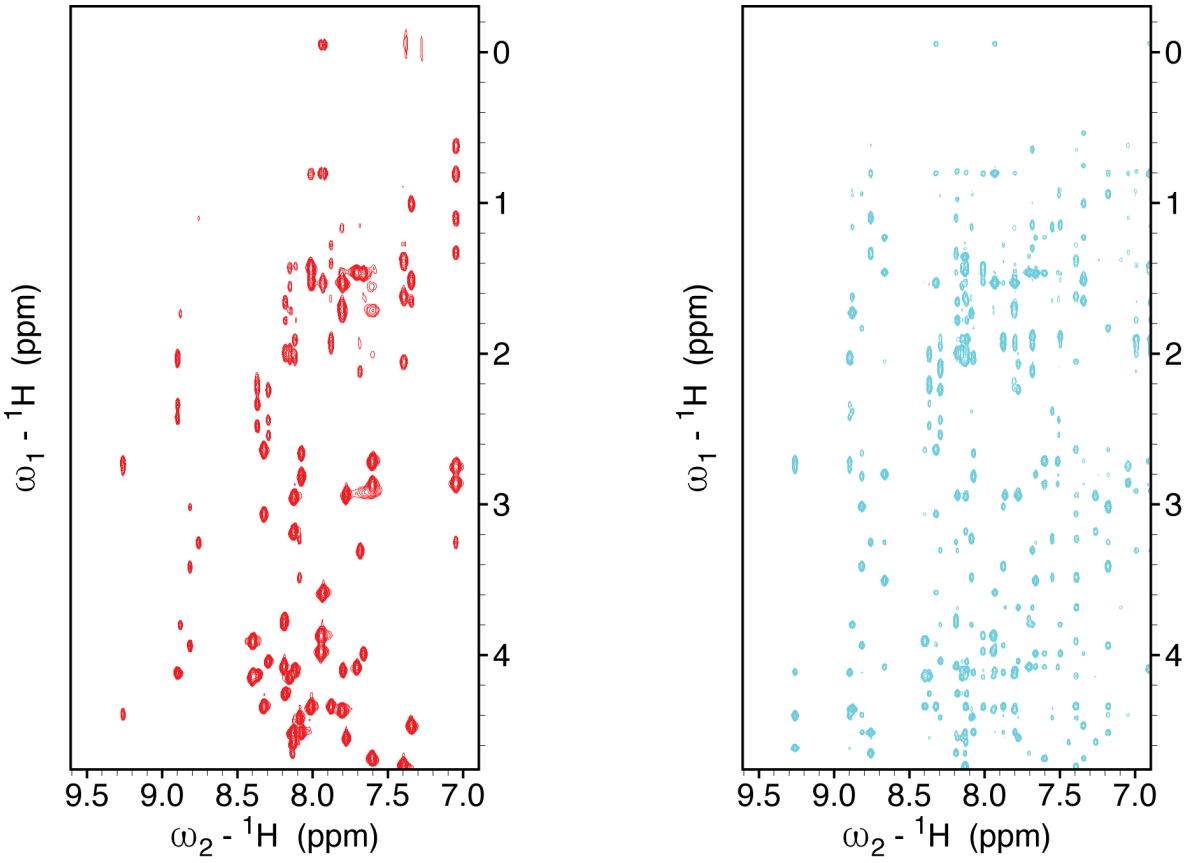

Figure S25. Views of the amide/aromatic to aliphatic region from TOCSY (left) and NOESY (right) spectra of **α^{Me}F17**.

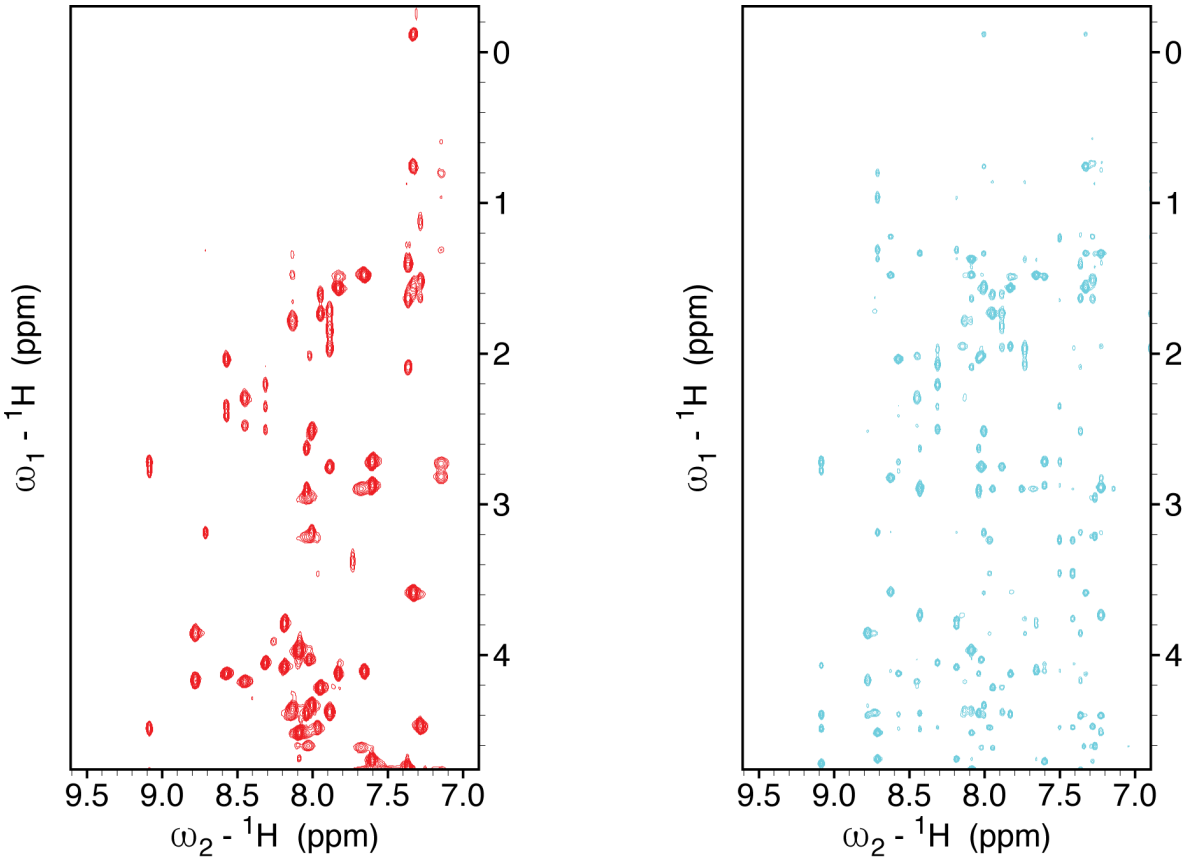

Figure S26. Views of the amide/aromatic to aliphatic region from TOCSY (left) and NOESY (right) spectra of triple substitution variant **α^{Me}F6/α^{Me}F17/ACPC29**.

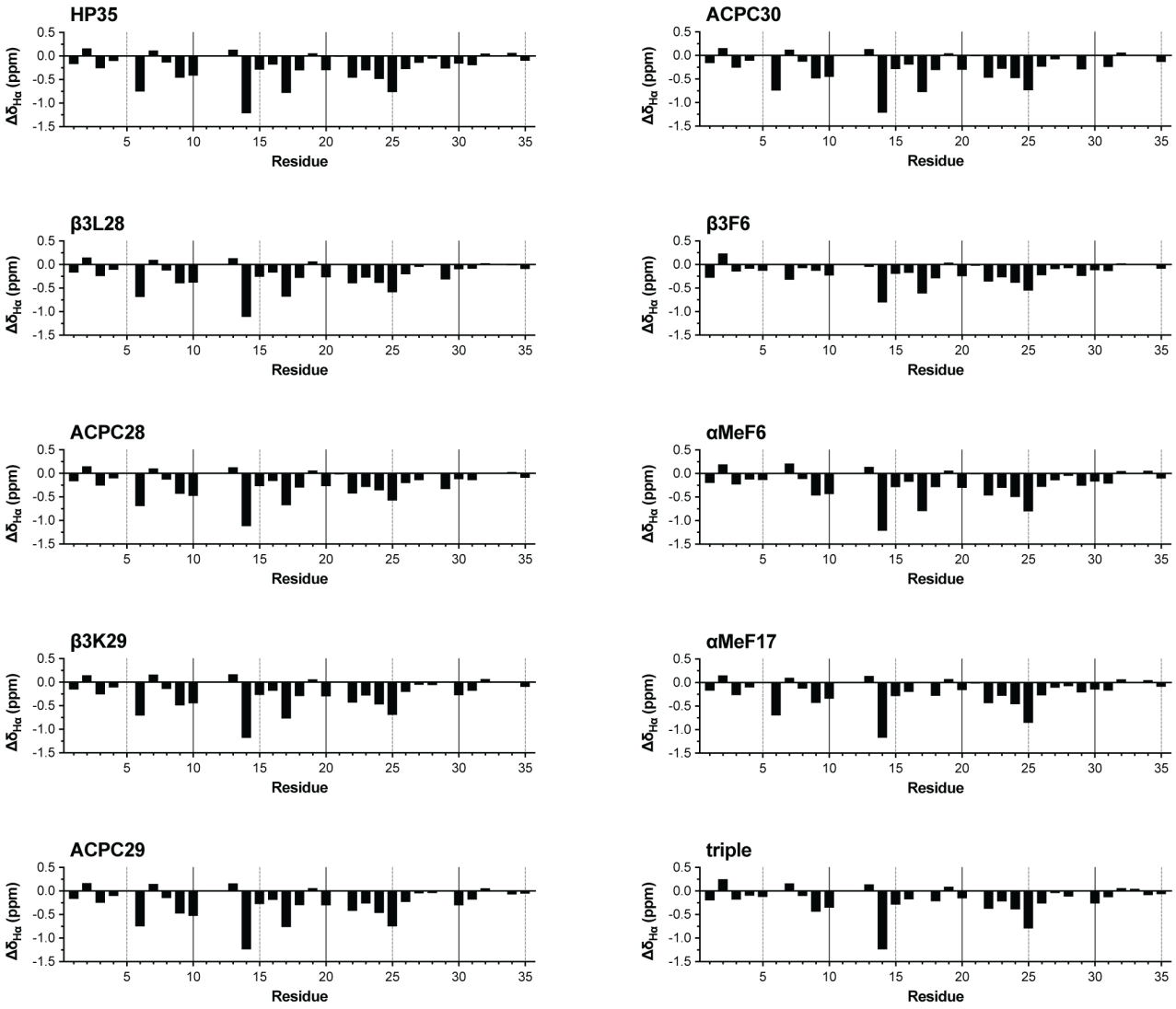

Figure S27. Chemical shift deviation of observed backbone H_α resonance frequency from calculated random coil values ($\Delta\delta H_\alpha$) for **HP35** and variants.[11,12] Data for **HP35** are previously published[10] and included here for comparison.

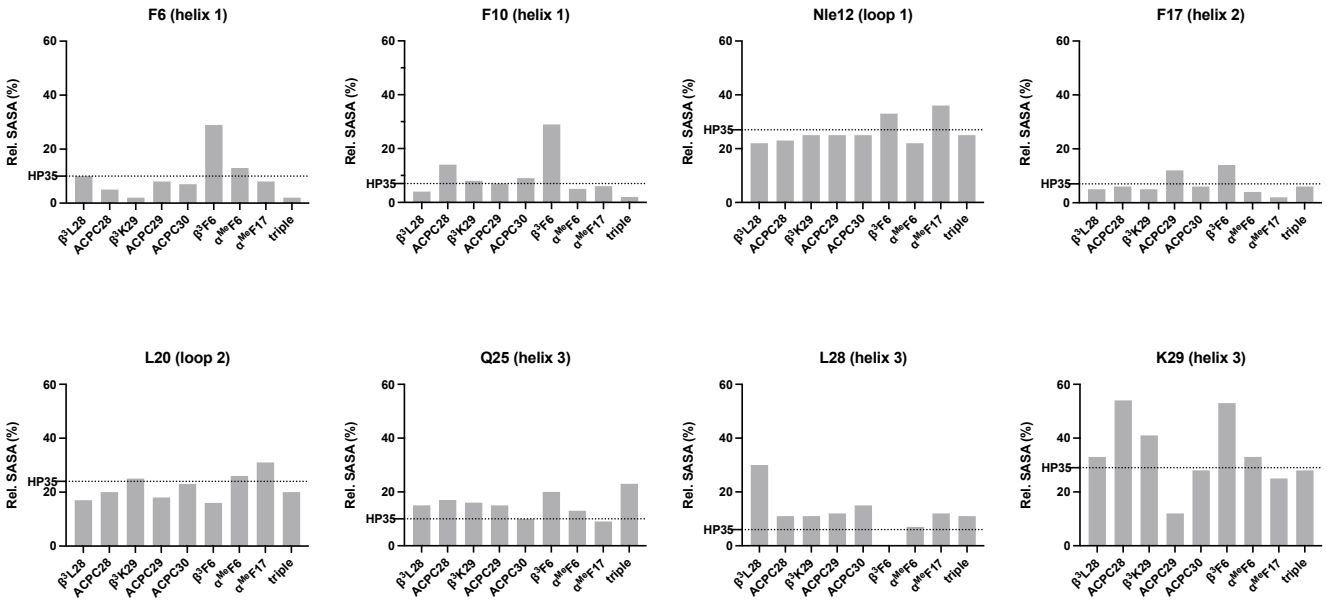

Figure S28. Relative solvent accessible surface area (rel. SASA) of buried/partially buried residues computed using Pymol for **HP35** and variants. The dashed line in each graph represents the rel. SASA value for that residue in **HP35**.

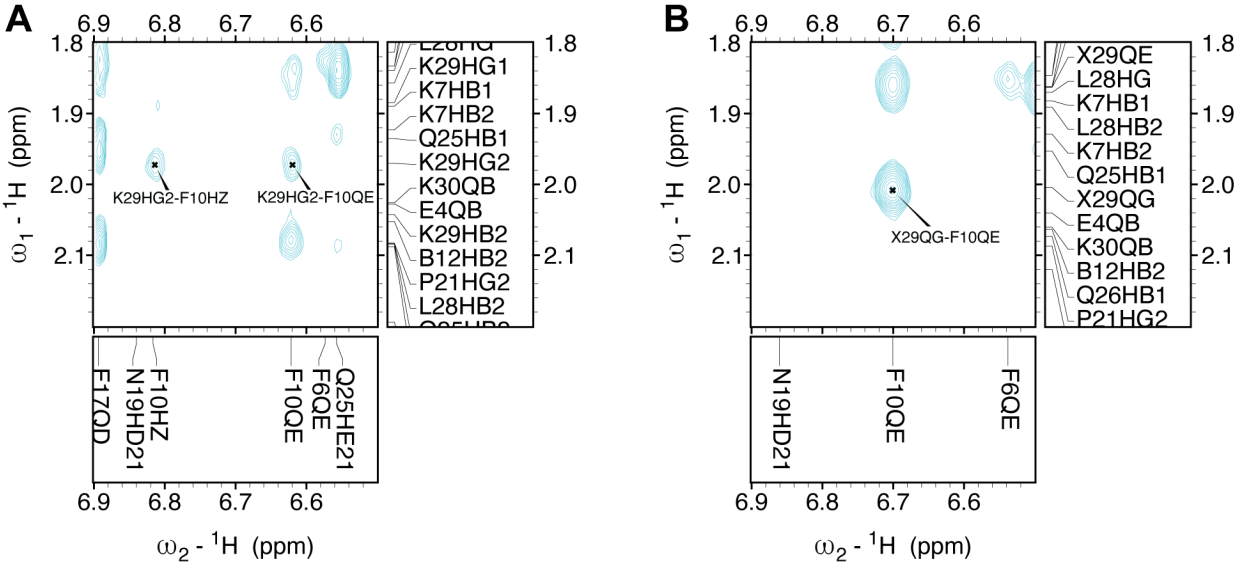

Figure S29. Views from the NOESY spectra of **HP35** (A) and variant **ACPC29** (B) showing peaks for well-resolved NOE correlations between the side chains of residues 29 and 10.

Table S1. Statistics from NMR structure calculation for **β³L28**.

	β³L28
Accession codes	
PDB	9YLZ
BMRB	31270
Experimental restraints	
Total NOEs	909
Unambiguous NOEs	745
Intra-residue	353
Sequential ($\|i - j\| = 1$)	140
Medium-range ($1 < \|i - j\| < 5$)	133
Long-range ($\|i - j\| \geq 5$)	119
Ambiguous NOEs	164
H-bonds	36
Violations	
NOE >0.5 Å	11.8 ± 4.7
NOE rmsd (Å)	0.11 ± 0.02
H-bond >0.5 Å	2.7 ± 2.3
Ensemble rmsd	
Backbone heavy atoms	0.80 ± 0.17
All heavy atoms	1.06 ± 0.17
Geometry analysis	
rmsd bonds (Å)	0.0033 ± 0.00012
rmsd angles (°)	0.47 ± 0.01
rmsd impropers (°)	1.2 ± 0.08
Ramachandran analysis	
Favored (%)	89.7
Allowed (%)	4.7
Disallowed (%)	5.6

Table S2. Statistics from NMR structure calculation for **ACPC28**.

	ACPC28
Accession codes	
PDB	9YM0
BMRB	31271
Experimental restraints	
Total NOEs	760
Unambiguous NOEs	640
Intra-residue	324
Sequential ($\|i - j\| = 1$)	115
Medium-range ($1 < \|i - j\| < 5$)	103
Long-range ($\|i - j\| \geq 5$)	98
Ambiguous NOEs	120
H-bonds	34
Violations	
NOE >0.5 Å	9.0 ± 1.7
NOE rmsd (Å)	0.10 ± 0.01
H-bond >0.5 Å	0 ± 0
Ensemble rmsd	
Backbone heavy atoms	0.41 ± 0.10
All heavy atoms	0.84 ± 0.06
Geometry analysis	
rmsd bonds (Å)	0.0028 ± 0.00010
rmsd angles (°)	0.43 ± 0.01
rmsd impropers (°)	1.2 ± 0.09
Ramachandran analysis	
Favored (%)	97.8
Allowed (%)	2.2
Disallowed (%)	0

Table S3. Statistics from NMR structure calculation for **β³K29**.

	β³K29
Accession codes	
PDB	9YM1
BMRB	31272
Experimental restraints	
Total NOEs	857
Unambiguous NOEs	738
Intra-residue	374
Sequential ($\|i - j\| = 1$)	141
Medium-range ($1 < \|i - j\| < 5$)	122
Long-range ($\|i - j\| \geq 5$)	101
Ambiguous NOEs	119
H-bonds	26
Violations	
NOE >0.5 Å	10.7 ± 1.8
NOE rmsd (Å)	0.12 ± 0.02
H-bond >0.5 Å	0 ± 0
Ensemble rmsd	
Backbone heavy atoms	0 .71 ± 0.26
All heavy atoms	0.96 ± 0.19
Geometry analysis	
rmsd bonds (Å)	0.0031 ± 0.00007
rmsd angles (°)	0.45 ± 0.02
rmsd impropers (°)	1.24 ± 0.08
Ramachandran analysis	
Favored (%)	95
Allowed (%)	5
Disallowed (%)	0

Table S4. Statistics from NMR structure calculation for **ACPC29**.

	ACPC29
Accession codes	
PDB	9YM2
BMRB	31273
Experimental restraints	
Total NOEs	885
Unambiguous NOEs	780
Intra-residue	379
Sequential ($\|i - j\| = 1$)	149
Medium-range ($1 < \|i - j\| < 5$)	135
Long-range ($\|i - j\| \geq 5$)	117
Ambiguous NOEs	105
H-bonds	26
Violations	
NOE >0.5 Å	7.9 ± 3.8
NOE rmsd (Å)	0.10 ± 0.02
H-bond >0.5 Å	0 ± 0
Ensemble rmsd	
Backbone heavy atoms	0.47 ± 0.12
All heavy atoms	0.72 ± 0.08
Geometry analysis	
rmsd bonds (Å)	0.0029 ± 0.00009
rmsd angles (°)	0.46 ± 0.01
rmsd impropers (°)	1.31 ± 0.10
Ramachandran analysis	
Favored (%)	96.9
Allowed (%)	3.1
Disallowed (%)	0

Table S5. Statistics from NMR structure calculation for **ACPC30**.

	ACPC30
Accession codes	
PDB	9YM3
BMRB	31274
Experimental restraints	
Total NOEs	788
Unambiguous NOEs	663
Intra-residue	348
Sequential ($\|i - j\| = 1$)	125
Medium-range ($1 < \|i - j\| < 5$)	104
Long-range ($\|i - j\| \geq 5$)	86
Ambiguous NOEs	125
H-bonds	26
Violations	
NOE >0.5 Å	5.8 ± 1.6
NOE rmsd (Å)	0.09 ± 0.02
H-bond >0.5 Å	0 ± 0
Ensemble rmsd	
Backbone heavy atoms	0.53 ± 0.16
All heavy atoms	0.93 ± 0.06
Geometry analysis	
rmsd bonds (Å)	0.0028 ± 0.00010
rmsd angles (°)	0.45 ± 0.01
rmsd impropers (°)	1.1 ± 0.06
Ramachandran analysis	
Favored (%)	95.9
Allowed (%)	4.1
Disallowed (%)	0

Table S6. Statistics from NMR structure calculation for **β³F6**.

	β³F6
Accession codes	
PDB	9YM4
BMRB	31275
Experimental restraints	
Total NOEs	698
Unambiguous NOEs	589
Intra-residue	331
Sequential ($\|i - j\| = 1$)	131
Medium-range ($1 < \|i - j\| < 5$)	91
Long-range ($\|i - j\| \geq 5$)	36
Ambiguous NOEs	109
H-bonds	30
Violations	
NOE >0.5 Å	15.1 ± 3.0
NOE rmsd (Å)	0.18 ± 0.05
H-bond >0.5 Å	8.4 ± 1.3
Ensemble rmsd	
Backbone heavy atoms	0.94 ± 0.24
All heavy atoms	1.27 ± 0.23
Geometry analysis	
rmsd bonds (Å)	0.0029 ± 0.00013
rmsd angles (°)	0.44 ± 0.01
rmsd impropers (°)	1.05 ± 0.09
Ramachandran analysis	
Favored (%)	86.9
Allowed (%)	11.5
Disallowed (%)	1.6

Table S7. Statistics from NMR structure calculation for **α^{Me}F6**.

	α^{Me}F6
Accession codes	
PDB	9YM5
BMRB	31276
Experimental restraints	
Total NOEs	929
Unambiguous NOEs	798
Intra-residue	369
Sequential ($\|i - j\| = 1$)	156
Medium-range ($1 < \|i - j\| < 5$)	156
Long-range ($\|i - j\| \geq 5$)	117
Ambiguous NOEs	131
H-bonds	32
Violations	
NOE >0.5 Å	5.6 ± 1.5
NOE rmsd (Å)	0.08 ± 0.01
H-bond >0.5 Å	0 ± 0
Ensemble rmsd	
Backbone heavy atoms	0.35 ± 0.16
All heavy atoms	0.71 ± 0.15
Geometry analysis	
rmsd bonds (Å)	0.0029 ± 0.00010
rmsd angles (°)	0.46 ± 0.02
rmsd impropers (°)	1.1 ± 0.07
Ramachandran analysis	
Favored (%)	97.2
Allowed (%)	2.5
Disallowed (%)	0.3

Table S8. Statistics from NMR structure calculation for **α^{Me}F17**.

	α^{Me}F17
Accession codes	
PDB	9YM6
BMRB	31277
Experimental restraints	
Total NOEs	
Unambiguous NOEs	819
Intra-residue	356
Sequential ($\|i - j\| = 1$)	167
Medium-range ($1 < \|i - j\| < 5$)	161
Long-range ($\|i - j\| \geq 5$)	136
Ambiguous NOEs	106
H-bonds	34
Violations	
NOE >0.5 Å	10 ± 1.7
NOE rmsd (Å)	0.12 ± 0.02
H-bond >0.5 Å	0 ± 0
Ensemble rmsd	
Backbone heavy atoms	0.32 ± 0.12
All heavy atoms	0.63 ± 0.10
Geometry analysis	
rmsd bonds (Å)	0.0028 ± 0.00007
rmsd angles (°)	0.43 ± 0.02
rmsd impropers (°)	1.3 ± 0.08
Ramachandran analysis	
Favored (%)	93.8
Allowed (%)	4
Disallowed (%)	2.2

Table S9. Statistics from NMR structure calculation for **α^{Me}F6/α^{Me}F17/ACPC29**.

	α^{Me}F6/α^{Me}F17/ACPC29
Accession codes	
PDB	9YM7
BMRB	31278
Experimental restraints	
Total NOEs	850
Unambiguous NOEs	663
Intra-residue	298
Sequential ($\|i - j\| = 1$)	143
Medium-range ($1 < \|i - j\| < 5$)	127
Long-range ($\|i - j\| \geq 5$)	95
Ambiguous NOEs	187
H-bonds	30
Violations	
NOE >0.5 Å	10.3 ± 3.5
NOE rmsd (Å)	0.11 ± 0.03
H-bond >0.5 Å	0 ± 0
Ensemble rmsd	
Backbone heavy atoms	0.57 ± 0.30
All heavy atoms	0.86 ± 0.26
Geometry analysis	
rmsd bonds (Å)	0.0028 ± 0.00009
rmsd angles (°)	0.49 ± 0.01
rmsd impropers (°)	1.1 ± 0.06
Ramachandran analysis	
Favored (%)	90.7
Allowed (%)	4.6
Disallowed (%)	4.7

References

1 S. C. Gill and P. H. v. Hippel, *Anal. Biochem.*, 1989, **182**, 319-326.
2 D. Shortle, A. K. Meeker and E. Freire, *Biochemistry*, 1988, **27**, 4761-4768.
3 M. M. Santoro and D. W. Bolen, *Biochemistry*, 1988, **27**, 8063-8068.
4 M. M. Santoro and D. W. Bolen, *Biochemistry*, 1988, **27**, 8063-8068.
5 W. Lee, M. Rahimi, Y. Lee and A. Chiu, *Bioinformatics*, 2021, **37**, 3041-3042.
6 W. Rieping, M. Habeck, B. Bardiaux, A. Bernard, T. E. Malliavin and M. Nilges, *Bioinformatics*, 2007, **23**, 381-382.
7 A. T. Brunger, *Nat. Protoc.*, 2007, **2**, 2728-2733.
8 J. P. Linge, M. Habeck, W. Rieping and M. Nilges, *J. Magn. Reson.*, 2004, **167**, 334-342.
9 F. Mareuil, T. E. Malliavin, M. Nilges and B. Bardiaux, *J. Biomol. NMR*, 2015, **62**, 425-438.
10 T. W. Harmon, Y. Lin, R. T. Sutton, S. W. J. Osborne and W. S. Horne, *ChemBioChem*, 2025, **26**, e202401022.
11 M. Kjaergaard and F. M. Poulsen, *J. Biomol. NMR*, 2011, **50**, 157-165.
12 Poulsen IDP/IUP random coil chemical shift server, https://spin.niddk.nih.gov/bax/nmrserver/Poulsen_rc_CS/.